Polarization transfer in quasifree $(\vec{p},\vec{n})$ reactions at 495 MeV

X. Y. Chen,[1] T. N. Taddeucci,[2] J. B. McClelland,[2] T. A. Carey,[2]
R. C. Byrd,[2] L. J. Rybarcyk,[2] W. C. Sailor,[2] D. J. Mercer,[1] D. L. Prout,[1]
S. DeLucia,[3] B. Luther,[3] D. G. Marchlenski,[3] E. Sugarbaker,[3]
J. Rapaport,[4] E. Gülmez,[5] C. A. Whitten, Jr.,[5] C. D. Goodman,[6]
W. Huang,[6] Y. Wang,[6] and W. P. Alford[7]

[1] *University of Colorado, Boulder, Colorado 80309*
[2] *Los Alamos National Laboratory, Los Alamos, New Mexico 87545*
[3] *The Ohio State University, Columbus, Ohio 43210*
[4] *Ohio University, Athens, Ohio 45701*
[5] *University of California, Los Angeles, California 90024*
[6] *Indiana University Cyclotron Facility, Bloomington, Indiana 47405*
[7] *University of Western Ontario, London, Ontario, Canada N6A 3K7*

(Received 22 January 1993)

A complete set of polarization-transfer observables has been measured for quasifree $(\vec{p},\vec{n})$ reactions on ^{2}H, ^{12}C, and ^{40}Ca at a bombarding energy of 495 MeV and a laboratory scattering angle of 18°. The data span an energy-loss range from 0 to 160 MeV, with a corresponding momentum transfer range of $q_{\rm c.m.} = 1.7$–1.9 fm^{-1}. The laboratory observables are used to construct partial cross sections proportional to the nonspin response and three orthogonal spin responses. These results are compared to the transverse spin response measured in deep inelastic electron scattering and to nuclear responses based on the random phase approximation. The polarization observables for all three targets are remarkably similar and reveal no evidence for an enhancement of the spin-longitudinal nuclear response relative to the spin-transverse response. These results suggest the need for substantial modifications to the standard form assumed for the residual particle-hole interaction.

PACS number(s): 25.40.Kv, 24.70.+s

I. INTRODUCTION

Isovector nuclear responses to mesonic fields are expected to show an enhanced ratio between the spin-longitudinal $(\boldsymbol{\sigma}\cdot\mathbf{q})$ and spin-transverse $(\boldsymbol{\sigma}\times\mathbf{q})$ response functions for momentum transfers $q \gtrsim 1$ fm^{-1}, as predicted by $\pi+\rho+g'$ mesonic-exchange models of the nuclear mean fields [1]. Measurements of polarization transfer in quasifree $(\vec{p},\vec{p}')$ reactions have been used to investigate these responses by a separation of the observed cross section into spin-longitudinal and spin-transverse channels. Unfortunately, this reaction does not distinguish between the isoscalar and isovector responses. The experimental capability now exists to investigate the spin responses using the purely isovector $(\vec{p},\vec{n})$ reaction. In this paper we present the results and analysis of the first such measurements.

The isovector spin-transverse response function has been investigated via deep inelastic electron scattering at several momentum transfers. Results have been reported by Barreau *et al.* [2] for the ^{12}C(e,e') response for 200 MeV/c < q < 600 MeV/c, by Deady *et al.* [3, 4] for the ^{40,48}Ca(e,e') responses for 250 MeV/c < q < 410 MeV/c, and by Meziani *et al.* [5] for the ^{40,48}Ca(e,e') and ^{56}Fe(e,e') responses for 300 MeV/c < q < 600 MeV/c. These results provide the clearest measure of the spin-transverse response function, partly because electrons penetrate the entire nuclear volume with little distortion. Although it is an ideal probe of the transverse response, inclusive electron scattering is not sensitive to the pionic spin-longitudinal response function.

While the spin-longitudinal response is expected to be important in $\Delta T = 1$ hadronic and semihadronic reactions, little is known experimentally about its shape and strength. For momentum transfers near the expected maximum of the longitudinal enhancement, only a few polarized-beam experiments sensitive to this component have been completed. The first measurements were those of Carey *et al.* for quasifree $(\vec{p},\vec{p}')$ scattering from ^{2}H, Ca, and Pb at 500 MeV [6, 7]. Measurements of quasifree $(\vec{p},\vec{p}')$ scattering from ^{2}H and ^{12}C have been reported by Fergerson *et al.* [8] for a bombarding energy of 800 MeV and laboratory scattering angles of 5°, 11°, and 20° (q = 0.6–2.5 fm^{-1}); however, these higher-energy measurements were primarily directed toward a study of the delta region of excitation. A measurement of ^{54}Fe$(\vec{p},\vec{p}')$ at 290 MeV and $q = 1.35$ fm^{-1} has been reported by Häusser *et al.* [9]. Finally, measurements of quasifree $(\vec{p},\vec{p}')$ scattering from ^{12}C at 290 MeV and 420 MeV and a momentum transfer of $q = 1.9$ fm^{-1} have been reported by Chan *et al.* [10]. Analyses of these measurements do not reveal the expected enhancement and softening of the spin-longitudinal response. However, interpretation of these results [11, 12] is problematic because the $(\vec{p},\vec{p}')$ reaction is not a pure $\Delta T = 1$ probe. A promising alternative probe, the tensor-polarized $(\vec{d},2p)$ reaction [13–15], appears to suffer from distortion effects that greatly dilute the sensitivity to differences between

the longitudinal and transverse channels [16]. The inherent ambiguities in the $(\vec{p},\vec{p}')$ data and the consequent importance of obtaining corresponding pure $\Delta T = 1$ data in the nuclear continuum region provided the motivation for the present experiment.

In this article, we report the first measurement of a complete set of polarization-transfer observables for quasifree $(\vec{p},\vec{n})$ reactions on ^{2}H, C, and Ca. The measurements were made at a bombarding energy of 495 MeV and a laboratory scattering angle of 18°, with a resultant momentum transfer of $q_{\rm lab} = 1.72$ fm^{-1} at the peak of the quasifree distribution. These correspond very closely to the kinematic conditions of the original $(\vec{p},\vec{p}')$ experiment [6, 7]. The measured polarization-transfer observables and cross sections are used to construct quantities proportional to the spin-longitudinal and spin-transverse responses. The effects of distortions and other reaction-mechanism complications are assessed by comparing the C and Ca results to the electron scattering responses and to the ^{2}H$(\vec{p},\vec{n})$ observables measured in this experiment. Finally, our results are compared to random phase approximation (RPA) responses that incorporate surface effects [17]. A brief description and analysis of the ratio of the $\Delta T = 1$ spin-longitudinal and spin-transverse responses R_L/R_T has been published in a previous Letter [18].

II. EXPERIMENTAL METHODS

The data presented here were obtained with the Neutron Time-of-Flight (NTOF) facility at the Clinton P. Anderson Meson Physics Facility (LAMPF) in Los Alamos. These data represent the first measurements of polarization-transfer observables with the NTOF facility. A detailed report concerning the calibration and operation of the detector system is in preparation. In the following sections we present a brief description of the detector system and discuss experimental details most relevant to the present experiment. A schematic layout of the pertinent beam lines, magnets, and detector system is presented in Figs. 1 and 2.

A. Proton beam

The polarized proton beam was provided by a new Optically Pumped Polarized Ion Source (OPPIS) [19]. The beam was delivered in macropulses with a length of approximately 725 μs and a repetition rate of 36 Hz. Within each macropulse, the beam was chopped and bunched to provide a separation between beam micropulses of 160/(805 MHz) = 198.8 ns. The polarization of the beam was cycled through the sequence (+,U,−,U) at 3 min intervals. The "+" and "−" are normal and reversed polarization states of the spin direction being delivered. The "U" state is unpolarized and comprised 16% of the

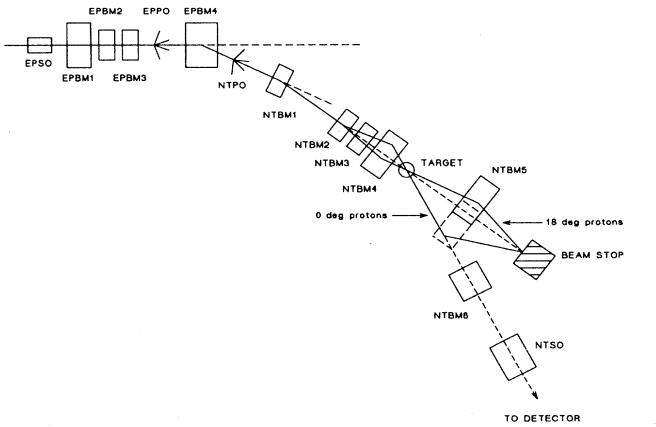

FIG. 1. Layout of important beam-line components (not to scale). The EP and NT beam lines are separated by a bend angle of 28°. The NT beam line bends by an additional angle of 5.5° at the NTBM1 magnet position. At the target position, the neutron flight path comes off at an angle of 12.5° with respect to the straight-through line to the beam stop. The solenoid magnet NTSO and sweep magnet NTBM6 are separated by a cylindrical iron neutron collimator imbedded in a concrete shield wall.

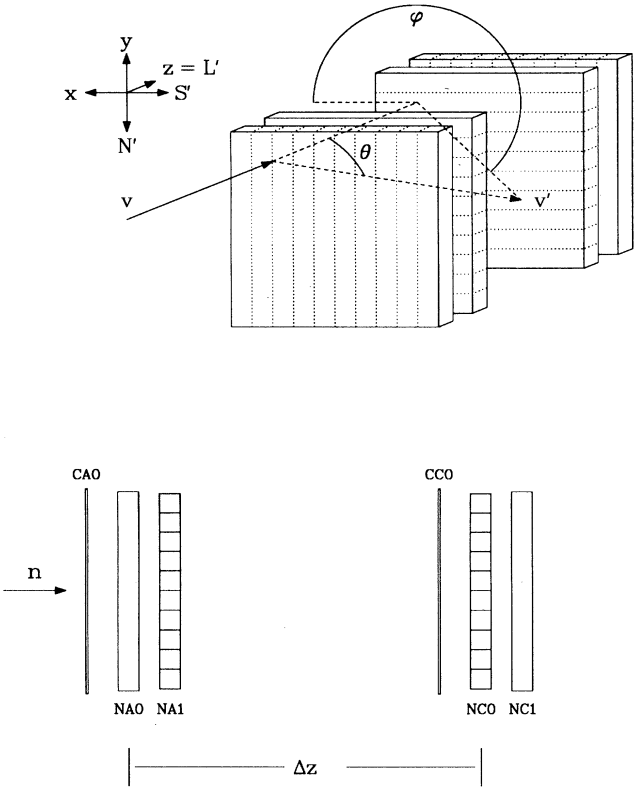

FIG. 2. Schematic of the NTOF detector system. The front pair of detector planes (NA0,NA1) serve as neutron polarization analyzers and are separated from the back pair of planes (NC0,NC1) by a distance of 1.4 m. Thin scintillators (CA0,CA1—not shown in the perspective view) are used to tag charged particles. The long axes of the detector cells in planes NA0 and NC1 are oriented vertically. The detector coordinate system (x,y,z) corresponds to the system $(-S',-N',L')$ for scattering to beam right.

beam polarization cycle. The beam energy was 495 MeV with an average polarization of about 0.53 and an average intensity of 78 nA on target. The beam intensity and polarization orientation are controlled by devices in the EP (external proton) beam line. A variable-aperture stripper at the entrance to the EP beam line was used to select the central portion of the beam (unstripped H^- ions) for transmission to the NTOF target. A superconducting solenoid (EPSO) was used both independently and in conjunction with three dipole magnets (EPBM1–3) to precess the proton beam polarization in the EP beam line to produce the desired orientation at the target position in the NT beam line.

The proton beam polarization was measured by beamline polarimeters at the exit of the EP beam line (EPPO) and entrance to the NT beamline (NTPO). These polarimeters are separated by a bend angle of 28°, thus allowing determination of both the horizontal and vertical beam polarizations and the total polarization vector. Each polarimeter consists of four arms of collimated pairs of conjugate-angle plastic-scintillator telescopes that continuously monitor the beam polarization via *pp* scattering from thin CH_2 targets. Systematic checks of the polarization measurements were made for a wide range of beam intensities, and comparisons of the total polarization for horizontally and vertically polarized beams showed excellent agreement. The systematic uncertainty in the total polarization is estimated to be about 0.01 [20], and statistical uncertainties were typically an order of magnitude smaller than this.

The polarized beam is fully stripped to positive protons by a thin foil between the precession magnets EPBM1 and EPBM2. From this point the horizontal component of the polarization vector precesses by an amount proportional to and in the same direction as the net bend angle. This proportionality is given by

$$\theta_{\rm prec} = \frac{T+m}{m}\left(\frac{g_p}{2}-1\right)\theta_{\rm bend}\ , \qquad (1)$$

where T is the kinetic energy of the beam, m is the proton mass, and $g_p/2 = 2.793$. For 495 MeV protons, this becomes $\theta_{\rm prec} = 2.74\theta_{\rm bend}$. The uncertainty in the horizontal polarization components at the target is determined by the uncertainty in the net bend angle. As indicated in Fig. 1, there are two bends in the beam line (28° at EPBM4, 5.5° at NTBM1), each with an uncertainty of $\lesssim 0.1°$. The remaining contribution to the uncertainty in the net bend angle is the uncertainty of the angle of incidence on the NTOF target. This angle is measured during the angle-setting procedure by two position-sensitive ion chambers on each side of the target. The size of the beam spot on target is typically about 1 cm, and the centroid of this distribution can be determined to an accuracy of about 1 mm. The separation between chambers is 61 cm. The resulting uncertainty in the scattering angle is therefore about 0.13°. Combining this, the beam-line uncertainties, and an uncertainty of about 0.1° in the mechanical alignment of the scattering-angle readout, the resulting uncertainty in the net bend angle is about 0.2°, and the uncertainty in the net precession angle is therefore about 0.6°.

B. Targets

Targets for the quasifree $(\vec{p},\vec{n})$ measurements included CD_2, natural C (98.9% ^{12}C), and natural Ca (96.9% ^{40}Ca) with areal densities of 0.99 g/cm^2 for carbon, 1.00 g/cm^2 for calcium, and 0.78 g/cm^2 for CD_2. For the present purpose, the natural carbon and calcium targets may be regarded as ^{12}C and ^{40}Ca. Additional calibration measurements at a scattering angle of 0° were made with targets of ^{14}C, ^{7}Li (0.73 g/cm^2), and CD_2. The ^{14}C target consisted of 170 mg/cm^2 of carbon (89% ^{14}C) encased in a nickel cell of 89 mg/cm^2 total thickness.

C. Neutron detector/polarimeter

High-resolution measurements of polarization transfer in $(\vec{p},\vec{n})$ reactions commenced at the Indiana University Cyclotron Facility (IUCF) in 1982, and many of the techniques developed there [21] have been scaled up and applied to the NTOF facility at LAMPF [22]. Improvements to the detector system include increased scintillator volume, the capability to simultaneously measure two orthogonal polarization directions, and continuous monitoring and calibration of the system by tracking cosmic-ray muons. The NTOF detector/polarimeter is illustrated schematically in Fig. 2. The detector consists of four parallel "planes" (NA0,NA1,NC0,NC1) oriented perpendicular to the incident neutron flux: three stainless-steel tanks filled with liquid scintillator (BC-517s, H:C=1.7) and a fourth set of ten plastic scintillators (BC-408). The liquid-scintillator tanks are each subdivided into ten optically isolated cells with dimensions of $10 \times 10 \times 107$ cm^3. The plastic-scintillator cells have the same dimensions. The detector cells are viewed on each end by phototubes coupled through lucite light guides. Thin plastic scintillators (CA0,CC0) in front of and between the front and back pairs of neutron detectors are used to tag charged particles. The relative timing and phototube gains of the entire detector array are continuously monitored and calibrated by tracking cosmic-ray muons. This procedure yields an intrinsic time resolution of about 300 ps (FWHM) and a long-term and short-term (1 h) pulse-height gain stability of about 2%. Position resolution along the long axis of each detector cell is about 4 cm (FWHM).

Incident neutron energy is determined by time of flight (TOF) to the front detector planes with respect to a rf stop signal derived from the linac. A strong gamma peak from π^0 production in the target provided a convenient time reference for establishing the absolute TOF scale. Transitions to discrete states with known reaction Q values then provided the absolute energy scale. The mean beam energy (target center) was thus determined to be 495 ± 0.5 MeV. The neutron flight path was 200 m for the quasifree measurements reported here. Additional measurements used to calibrate the effective analyzing power of the detector for polarimetry were made on a flight path of 400 m. In both cases time and energy spread in the beam were minimized with a rebunching technique that employs nonaccelerating rf cavities in the linac [23]. Energy resolution for the quasifree measure-

ments was approximately 2 MeV (including target energy loss contributions) and was about 0.75 MeV for the calibration measurements on the longer flight path.

In polarimetry mode, the front pair of liquid-scintillator planes also serve as neutron polarization analyzers. Time, position, and pulse-height information from front and back planes are used to kinematically select $n+p$ interactions. This kinematic selection also provides a highly efficient filter against background events from cosmic rays, target gamma rays, or slow neutrons from preceding beam bursts. Neutron polarization is determined from the azimuthal intensity distribution of the $n+p$ events. Elastic $^1\mathrm{H}(\vec{n},n)$ and charge-exchange $^1\mathrm{H}(\vec{n},p)$ events are identified and sorted separately. Because of energy-resolution limitations in the interplane timing, quasifree n+C events also contribute to both of these reaction channels. The similar analyzing powers and larger cross sections of the quasifree reactions result in an important beneficial contribution to the detection efficiency of the system. While the qualitative response (efficiency and analyzing power) of the polarimeter can be modeled using free nucleon-nucleon observables, the significant contribution of quasifree scattering makes it necessary to empirically calibrate the polarimeter rather than rely on Monte Carlo simulations.

D. Effective analyzing power

The magnitude and energy dependence of the effective analyzing power for each reaction channel in the polarimeter have been determined by observing neutrons produced by three different source reactions: $^2\mathrm{H}(\vec{p},\vec{n})$ at 0°, $^2\mathrm{H}(\vec{p},\vec{n})$ at 18°, and $^{14}\mathrm{C}(\vec{p},\vec{n})^{14}\mathrm{N}(2.31\ \mathrm{MeV})$ at 0°. The effective analyzing powers derived from these measurements are displayed in Fig. 3.

The 0° measurements used a longitudinally polarized beam (along the beam momentum) to produce longitudinally polarized neutrons. The $0^+ \rightarrow 0^+$ $^{14}\mathrm{C}(\vec{p},\vec{n})$ isobaric analog state reaction produces neutrons at zero degrees that have the same polarization as the incident proton beam. This reaction provided a calibration for a neutron energy of 492 MeV. The longitudinal polarization transfer for the $^2\mathrm{H}(\vec{p},\vec{n})$ reaction at 0° has been measured independently by McNaughton *et al.* for proton energies between 305 MeV and 788 MeV [24]. This reaction was used at bombarding energies of 495 MeV and 318 MeV to produce calibrations for average neutron energies near 489 MeV and 312 MeV, respectively. At scattering angles substantially larger than 0°, the spectrum of neutrons produced in the $^2\mathrm{H}(\vec{p},\vec{n})$ reaction consists primarily of a broad quasifree distribution. The identity between the induced polarization and analyzing power, $P = A_y$, that applies in free scattering should hold to a high degree of accuracy for these quasifree neutrons. This relation has been used to obtain a calibration for neutron energies near 435 MeV, corresponding to the peak of the $^2\mathrm{H}(\vec{p},\vec{n})$ quasifree distribution for a bombarding energy of 495 MeV and a scattering angle of 18°.

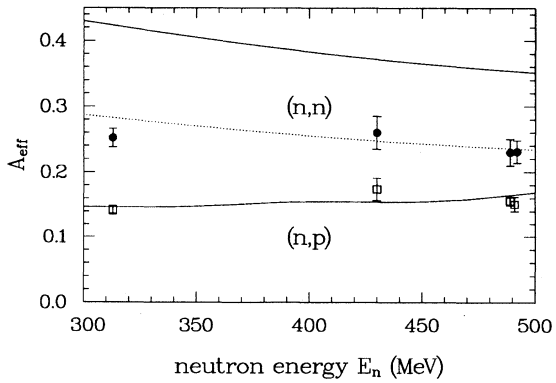

FIG. 3. Effective analyzing power for the NTOF detector in the (n,n) (solid circles) and (n,p) (boxes) reaction channels. The solid lines represent Monte Carlo calculations employing free np observables. The dashed line is the (n,n) calculation normalized by 2/3.

The magnitude of the effective analyzing power in each channel was determined in two steps. First, the analyzing-power ratio between the two channels was established from all available data. Next, with this ratio fixed to the value found in the first step, the weighted average of the two channels was normalized to the CD_2 and $^{14}\mathrm{C}$ calibration data. The resulting statistical uncertainty in the overall normalization factor is about 7% at 492 MeV and about 5% at 312 MeV. This statistical calibration uncertainty represents the systematic uncertainty in the independent measurements of the quasifree neutron polarization.

E. Data acquisition and event rates

Time and pulse-height information were digitized using LeCroy FERA (fast encoding and readout ADC) ADC and TFC (time-to-FERA converter) modules. Nonzero data words were written to a FERA fast-memory module during beam macropulses and then transferred to magnetic tape between macropulses. No digital event filtering was used online. Overall rates were reduced by imposing a time window on the triggers corresponding to neutron-induced events. This window limited the range of accepted neutron energies to a maximum energy loss of about 160 MeV. Events within this time window that produced hits in only the front or back pair of detector planes were further prescaled by a factor of 500. With the time windows and event prescaling in effect, typical event rates for the quasifree measurements with 80 nA of beam were 800 Hz with a corresponding system livetime of about 45%.

F. Detector efficiency and cross section normalization

The detection efficiency was determined by normalizing to neutron yields from the $^7\mathrm{Li}(p,n)^7\mathrm{Be}$(g.s.+0.43 MeV) reaction, which has a constant c.m. cross section of $\sigma(0°) = 27.0 \pm 0.8$ mb/sr [25]. This reaction was used at bombarding energies of 495 MeV and 318 MeV to pro-

duce an efficiency calibration spanning the range of the present data. The detection efficiency in the polarimetry mode was found to be almost independent of energy, with a value of approximately 0.75% for the combined (n,n) and (n,p) channels. Beam current was measured by integrating the output from a secondary-emission monitor upstream from the target, and by integrating the charge collected in the beam stop, which consists of electrically insulated graphite blocks. The ratio of integrated charges observed with these two devices was stable to within a standard deviation of 3%. Combining this in quadrature with the uncertainty in the ^{7}Li cross section (3%) and the estimated uncertainty in target thicknesses (2%), we estimate a cross section normalization uncertainty of about 6%.

G. Neutron precession and spin reversals

Three separate magnets were used to reorient the outgoing neutron spin and to periodically reverse its direction in order to cancel false asymmetries in the detection system. A schematic layout of the beam-swinger and precession system is shown in Fig. 1. Four dipole magnets (NTBM1–4) with vertical fields were used to adjust the angle of incidence of the proton beam on the target. Magnets used to precess the neutron spin consisted of a dipole with a vertical field (NTBM5), a dipole with a horizontal field (NTBM6), and a superconducting solenoid (NTSO). The magnet NTBM5 also served as a clearing magnet to steer the unscattered proton beam into the beam stop, and magnet NTBM6 functioned as a sweep magnet to prevent charged reaction products from entering the neutron flight path.

For the calibration measurements at 0°, reversal of the proton spin exactly reversed the outgoing neutron spin. In this case the precession system was simply used to reorient the outgoing neutron polarization. Longitudinal polarization was first precessed by 45° in the horizontal plane as the neutrons passed through the field of NTBM5. The remaining longitudinal component was then precessed out of plane by 90° as the neutrons passed through the horizontal field of NTBM6. Outgoing longitudinal polarization at the target was therefore transformed into measurable transverse components at the detector.

Two different precession schemes were used for the measurements at a scattering angle of 18°. In both cases the clearing magnet NTBM5 was repositioned out of the neutron flight path and did not affect the neutron polarization. The fields of the precession magnets were set to provide optimum precession for neutrons of 420 MeV, which is near the peak of the quasifree distribution at this angle.

For sideways (S) and longitudinally (L) polarized beams, the horizontal dipole field of NTBM6 was used to precess the outgoing L component into N (normal to reaction plane) polarization at the detector. The outgoing S polarization was unaffected by this field, while the induced N-type polarization was precessed into unobservable L-type polarization at the detector. Reversal of the proton polarization thus reversed the remaining observable components of the neutron polarization. Because the only precession field used in this case was that of NTBM6, there was no precessional mixing between horizontal polarization components. The precession angle in a dipole field is proportional to $1/\beta$, so that lower-energy neutrons were overprecessed (96.3° at 335 MeV) and higher-energy neutrons were underprecessed (87.5° at 465 MeV) by small amounts. Corrections for this under- and overprecession were necessary to account for the small amount of mixing between N- and L-type polarization that occurred for neutrons with energies above and below the central value.

For a vertically (N) polarized beam, two precession magnets were used. The field in the sweep magnet NTBM6 was reduced to the minimum value consistent with its dual function. This field setting precessed 420 MeV neutrons by 25.8°, leaving 90% of the original outgoing N component. The superconducting solenoid NTSO was then used to precess this remaining N-type polarization alternately by ±90°. These reversals were initiated after accumulating a preset number of events, typically every few hours. Six (normal, reverse) cycles were completed for each target. The precession angle in a solenoidal field is proportional to $1/\beta\gamma$, so that 335 MeV neutrons were overprecessed (102.7°), and 465 MeV neutrons were underprecessed (84.7°). Corrections were applied for the precession deviations in both NTBM6 and NTSO.

III. DATA REDUCTION AND RESULTS

A. Coordinate system and observables

The three orthogonal components of the outgoing neutron polarization $\mathbf{p}' = (p_{S'}, p_{N'}, p_{L'})$ are related to the components of the incident proton polarization $\mathbf{p} = (p_S, p_N, p_L)$ through a set of polarization-transfer coefficients $D_{ij} (i = S', N', L', j = S, N, L)$ according to

$$\begin{pmatrix} p_{S'} \\ p_{N'} \\ p_{L'} \end{pmatrix} = \left[\begin{pmatrix} D_{S'S} & 0 & D_{S'L} \\ 0 & D_{N'N} & 0 \\ D_{L'S} & 0 & D_{L'L} \end{pmatrix} \begin{pmatrix} p_S \\ p_N \\ p_L \end{pmatrix} + \begin{pmatrix} 0 \\ P \\ 0 \end{pmatrix} \right] \frac{1}{1 + p_N A_y} . \quad (2)$$

This relation involves the complete set of polarization-transfer observables allowed for parity-conserving reactions. The sideways (S), normal (N), and longitudinal (L) coordinates are defined in terms of the proton momentum $\mathbf{k}_i$ and the neutron momentum $\mathbf{k}_f$ in the laboratory frame as $\hat{\mathbf{L}} = \hat{\mathbf{k}}_i$, $\hat{\mathbf{L}}' = \hat{\mathbf{k}}_f$, $\hat{\mathbf{N}} = \hat{\mathbf{N}}' = \hat{\mathbf{k}}_i \times \hat{\mathbf{k}}_f$, $\hat{\mathbf{S}} = \hat{\mathbf{N}} \times \hat{\mathbf{L}}$, and $\hat{\mathbf{S}}' = \hat{\mathbf{N}}' \times \hat{\mathbf{L}}'$. Note that an induced polarization component P can contribute to the outgoing

N-type neutron polarization regardless of the polarization of the incoming beam.

The polarization-transfer observables in Eq. (2) were determined by targeting approximately pure sideways (S), longitudinal (L), and normal (N) proton polarization components. Minor beam polarization components were less than 0.01 for S- and L-type beams, and a minor L-type component of about 0.035 was present for the measurements with an N-type beam. The effects of these minor components have been accounted for and included in all the values reported here. Measurements with L-type beams provided the coefficients $D_{L'L}$ and $D_{S'L}$, while S-type beams provided $D_{S'S}$ and $D_{L'S}$. The analyzing power A_y, induced polarization P, and polarization-transfer coefficient D_{NN} were obtained with an N-type beam, while an independent measurement of P was also obtained using the unpolarized (U) fraction of the beam. The values of P obtained with polarized and unpolarized beam are in excellent agreement, and serve to constrain several possible types of systematic error in the neutron polarization measurements.

B. Rate-dependent corrections

At high data rates, the low duty factor of the linac makes it necessary to correct for random coincidences in the polarimeters that mimic the double-scattering events of interest. Corrections to the rates measured in the beam-line polarimeters were made in a simple way by creating a parallel coincidence circuit in which one of the signals was delayed by an integral number of beam pulse periods. This allowed the random coincidence rate to be measured directly. This scheme is impractical for the neutron polarimeter, however, because of the more complicated acquisition electronics. Instead, a Monte Carlo simulation of the neutron-polarimeter geometry and event timing was used to calculate and correct for the rate of false coincidences.

Within the range of data rates encountered in the measurements reported here, only the (n,n) reaction channel in the neutron polarimeter was affected by false coincidences. The hardware trigger for (n,p) events was a threefold coincidence involving a charged-particle generated in the front pair of detectors. The thin scintillator used to generate the charged-particle trigger input has a very low efficiency for detecting neutrons. The rate of false threefold coincidences was therefore negligible, and was further reduced by software cuts.

It can be shown that the overall rate (probability per micropulse) of false coincidences in the (n,n) reaction channel is given by [26]

$$r_{\rm acc} = \mu^2(\varepsilon_F - \varepsilon_C)\varepsilon_B e^{-\mu\varepsilon_S} , \tag{3}$$

where ε_F and ε_B are the singles detection efficiencies of the front (F) and back (B) pair of detector planes, $\varepsilon_S = \varepsilon_F + \varepsilon_B$, ε_C is the detection efficiency for all events involving a coincidence between the front and back pair of planes, and μ is the probability of obtaining a neutron at the detector from a single beam burst. Typical values for the detection efficiencies are $\varepsilon_F = 0.15$, $\varepsilon_B = 0.10$, and $\varepsilon_C = 0.04$. The highest neutron rates during the quasifree measurements yielded a neutron probability of $\mu = 0.15$. The detection efficiency for the (n,n) channel was about 1.5×10^{-3} with all software cuts imposed. This implies a false/true coincidence ratio close to unity. Fortunately, this ratio is greatly reduced by the kinematic and angle cuts imposed in software. The most important of these software cuts involves the interplane velocity of the scattered neutrons. The fraction of false coincidences that pass this particular cut is dependent on the time distribution of the incident neutrons, and is highest when most of the rate is concentrated into a single peak of narrow time width. Quasifree (p,n) reactions at 18° produce neutrons that are well distributed in time; the fraction of false coincidences in the quasifree measurements that passed all cuts was typically only a few percent of the true coincidence rate. Test measurements with ^{7}Li and CD_2 targets at 0°, however, involved corrections as large as 20%. Measurements with these targets for rates that varied by an order of magnitude were well described by the Monte Carlo modeling. The much smaller corrections applied to the quasifree data should therefore be quite accurate.

C. ^{2}H$(\vec{p},\vec{n})$ observables

Observables for ^{2}H$(\vec{p},\vec{n})$ are obtained from a cross section weighted subtraction of the C observables from the CD_2 observables. A representative set of cross section spectra are shown in Fig. 4. The ^{2}H$(\vec{p},\vec{n})$ cross section is obtained from CD_2 and C according to

$$\sigma_{^2\rm H} = (\sigma_{\rm CD_2} - \sigma_{\rm C})/2 . \tag{4}$$

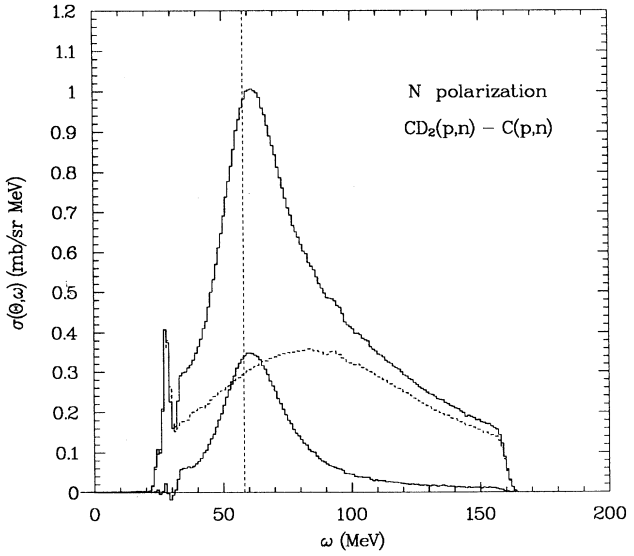

FIG. 4. Cross section spectra for (p,n) reactions on CD_2, C, and ^{2}H obtained with an N-type polarized beam. A dashed vertical line marks the energy loss for free np scattering.

Polarization observables are obtained from

$$D_{^2\mathrm{H}} = (D_{\mathrm{CD_2}} - f_{\mathrm{C}} D_{\mathrm{C}})/(1 - f_{\mathrm{C}}) \,, \tag{5}$$

where D represents one of the observables D_{ij}, P, or A, and $f_{\mathrm{C}} = \sigma_{\mathrm{C}}(\omega)/\sigma_{\mathrm{CD_2}}(\omega)$ is the carbon fraction of the CD_2 cross section for energy loss ω. An initial estimate of the carbon fraction was obtained with cross sections based on the nominal target thicknesses and integrated beam currents. The relative normalization for each incident spin state was then adjusted to produce the best subtraction of the peak at $\omega = 27.3$ MeV. This peak corresponds to the transition to the 4^- state at $E_x = 4.2$ MeV in ^{12}N. The normalization factors required for S-, N-, and L-type beams were 0.98, 1.00, and 1.04, respectively. This variation is consistent with the independently determined 3% beam-integration uncertainty. Following from these three normalization factors, a 2% systematic uncertainty in the carbon fraction has been included in the extraction of the $^2\mathrm{H}(\vec{p},\vec{n})$ observables.

Several features of the $^2\mathrm{H}(p,n)$ cross section spectrum are worth noting. The quasifree distribution has a width (FWHM) of about 28 MeV and peaks at an energy loss of 60 MeV. This is 2 MeV larger than the energy loss for free $n(p,n)p$ scattering; the Q value for the reaction $^2\mathrm{H}(p,n)2p$ is 2.2 MeV. A small peak near $\omega = 33$ MeV corresponds to the two-proton final state of the $^2\mathrm{H}(p,n)^2\mathrm{He}$ reaction. At small momentum transfer this reaction has a spin structure like that of a $1^+ \rightarrow 0^+$ reaction, and can therefore produce observables substantially different from those of free np scattering. In comparisons of the quasifree $^2\mathrm{H}(p,n)$ observables to those for free scattering, this region should therefore be avoided. Finally, as a check on the cross section normalization, we note that the $^2\mathrm{H}(p,n)$ cross section summed over the region $\omega = 30$–100 MeV is 11.5 mb/sr. This compares quite well to the phase-shift value of 11.6 mb/sr for free scattering [27].

D. Quasifree observables

The cross section, polarization, and analyzing power for ^{2}H, ^{12}C, and ^{40}Ca are presented in Fig. 5. Dotted vertical lines mark the energy loss for free np scattering. Note that the quasifree distribution for $^{12}\mathrm{C}(\vec{p},\vec{n})$ and $^{40}\mathrm{Ca}(\vec{p},\vec{n})$ peaks at an energy loss of about 80 MeV. This is 22 MeV larger than the energy loss for free scattering. The analyzing power and induced polarization are in very close agreement for the energy-loss region spanning the peak of the quasifree distributions. Solid horizontal lines represent optimal-frame free np values from the phase-shift solution of Bugg and Bryan [28]. Dashed horizontal lines correspond to the FA91 phase-shift solution of Arndt [27].

The diagonal polarization-transfer coefficients $D_{S'S}$, D_{NN}, and $D_{L'L}$ are presented in Fig. 6. The data here are binned in 10 MeV intervals. Dotted vertical lines mark the energy loss for free scattering. The solid horizontal lines represent the optimal-frame free np values from Bugg and Bryan [28]. The dashed lines correspond to values from the FA91 phase-shift solution of Arndt [27].

Tabulations of the data presented in Figs. 5 and 6 are given in Tables I–VI. The cross section, polarization, and analyzing power for each target are given in Tables I–III. Polarization-transfer coefficients are given in Tables IV–VI. All data are binned in 10 MeV intervals.

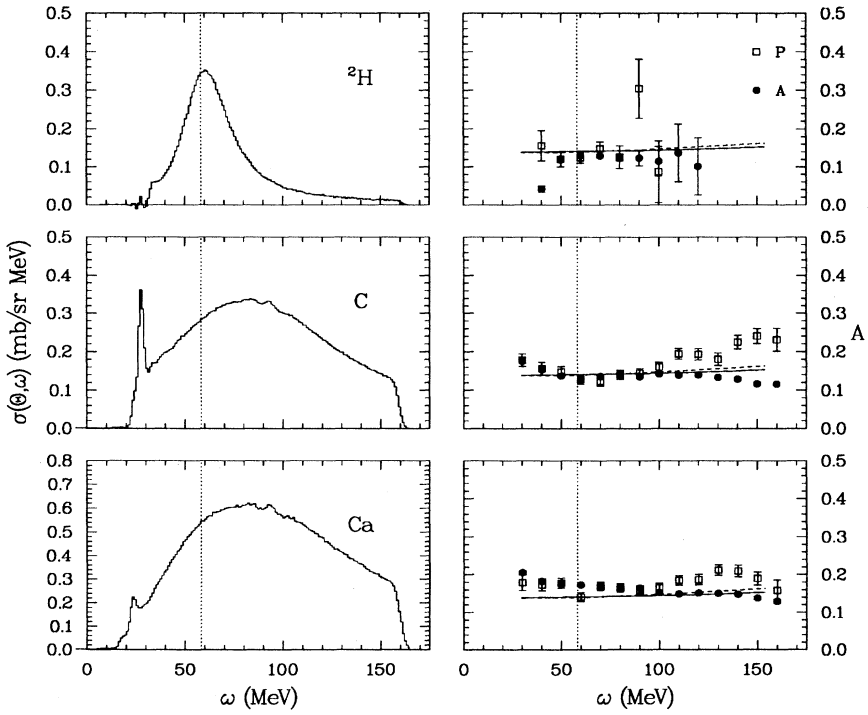

FIG. 5. Cross section, polarization, and analyzing power for ^{2}H, ^{12}C, and ^{40}Ca. The cross section is binned in 1 MeV steps. The polarization and analyzing power are binned in 10 MeV steps. The dotted vertical lines mark the energy loss for free np scattering. The solid horizontal lines represent the optimal-frame np values from the phase-shift solution of Bugg and Bryan [28]. The dashed horizontal lines are from the FA91 phase-shift solution of Arndt [27]. The small "wiggle" in the cross section spectra near $\omega = 90$ MeV is due to a differential nonlinearity in the TFC channel used to digitize the rf stop signal. This problem does not affect the polarization observables.

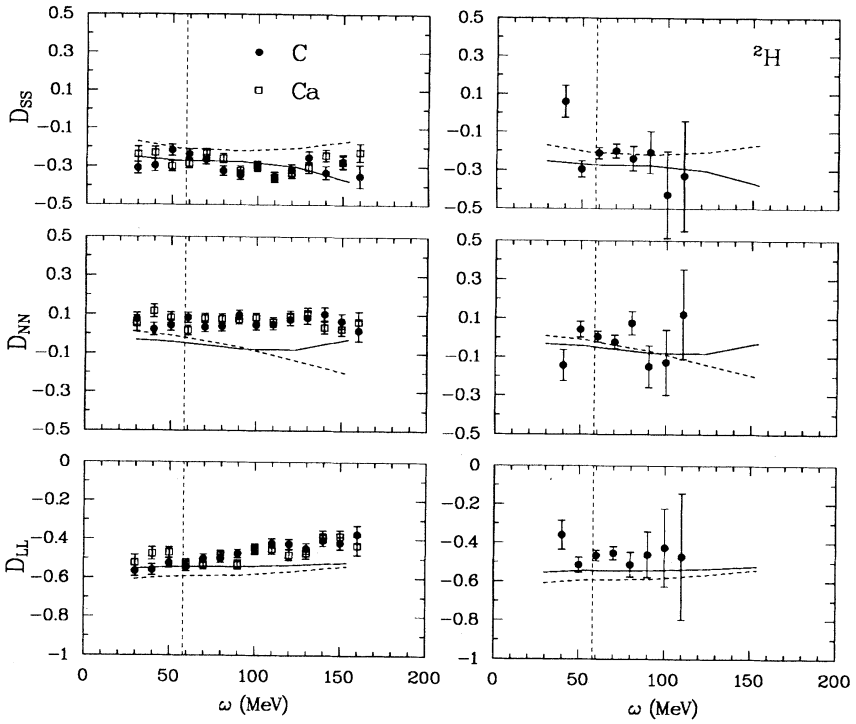

FIG. 6. Polarization-transfer coefficients D_{SS}, D_{NN}, and D_{LL} for ^{2}H, ^{12}C, and ^{40}Ca. The dashed vertical lines mark the energy loss for free np scattering. The solid horizontal lines represent the optimal-frame np values from the phase-shift solution of Bugg and Bryan [28]. The dashed horizontal lines are from the FA91 phase-shift solution of Arndt [27].

IV. DEFINITION OF THE EXPERIMENTAL NUCLEAR RESPONSES

In the one-photon-exchange model the inclusive cross section for deep inelastic electron-nucleus (eA) scattering is related to the longitudinal (charge) and transverse (spin and current) nuclear responses according to [29]

$$I^{eA}(q,\omega) = \frac{4\pi}{M_T}\sigma_M \{\lambda^2 S_L(q,\omega) + [\tfrac{1}{2}\lambda + \tan^2(\tfrac{\theta}{2})]S_T(q,\omega)\} , \quad (6)$$

where $I^{eA}(q,\omega) \equiv d^2\sigma/d\Omega\, d\omega$, $\lambda = 1 - \omega^2/q^2$, σ_M is the Mott cross section, and M_T is the initial target mass. The transverse structure function S_T represents the response to the spin-transverse operator $(\boldsymbol{\sigma} \times \mathbf{q})$ and can in principle be related to similar quantities measured with the $(\vec{p},\vec{n})$ reaction. In this latter case, the nucleon-nucleus (NA) double-differential cross section I^{NA} can be represented as a sum of terms [30–35]

$$I^{NA} = I_0 R_0 + I_q R_q + I_n R_n + I_p R_p , \quad (7)$$

where the I_i are nucleon-nucleon (NN) partial differential cross sections and the R_i are four response functions corresponding to the unit operator and three orthogonal spin operators. These four response functions can be separated by forming four polarization-transfer observables

TABLE I. Cross section (laboratory), polarization, and analyzing power for the ^{2}H$(\vec{p},\vec{n})$ reaction at 495 MeV and $\theta_{\rm lab} = 18°$. The uncertainties are from counting statistics and subtraction systematics.

ω (MeV)	$\sigma(\omega)$ [mb/(sr 10-MeV)]	A_y	P
100.0	0.4545±0.0039	0.115±0.039	0.087±0.081
90.0	0.7628±0.0042	0.124±0.021	0.305±0.076
80.0	1.3919±0.0045	0.125±0.009	0.126±0.030
70.0	2.5946±0.0051	0.129±0.004	0.148±0.018
60.0	3.4015±0.0053	0.129±0.003	0.124±0.014
50.0	2.1117±0.0045	0.119±0.004	0.120±0.019
40.0	0.8251±0.0035	0.041±0.008	0.156±0.040

TABLE II. Cross section (laboratory), polarization, and analyzing power for the ^{12}C$(\vec{p},\vec{n})$ reaction at 495 MeV and $\theta_{\rm lab} = 18°$. The uncertainties are from counting statistics only.

ω (MeV)	$\sigma(\omega)$ [mb/(sr 10-MeV)]	A_y	P
160.0	0.7005±0.0021	0.116±0.005	0.231±0.030
150.0	1.5515±0.0031	0.117±0.004	0.240±0.020
140.0	1.8260±0.0033	0.129±0.003	0.225±0.018
130.0	2.1435±0.0036	0.133±0.003	0.180±0.016
120.0	2.5326±0.0039	0.140±0.003	0.193±0.015
110.0	2.9191±0.0042	0.139±0.003	0.194±0.014
100.0	3.2680±0.0045	0.142±0.002	0.161±0.013
90.0	3.5369±0.0047	0.135±0.002	0.144±0.012
80.0	3.5813±0.0047	0.139±0.002	0.140±0.012
70.0	3.4150±0.0046	0.136±0.002	0.123±0.012
60.0	3.0694±0.0044	0.132±0.003	0.128±0.013
50.0	2.5896±0.0040	0.137±0.003	0.147±0.014
40.0	2.0604±0.0036	0.154±0.003	0.156±0.016
30.0	2.1975±0.0037	0.175±0.003	0.178±0.016

D_i that project out partial NA cross sections proportional to linear combinations of the responses. The $(\vec{p},\vec{n})$ responses are then derived from the four equations:

$$I_{\rm lab}^{NA} D_0 = C_K N_{\rm eff}(|\tilde{C}_2|^2 R_n + |\tilde{A}|^2 R_0) \ , \tag{8}$$

$$I_{\rm lab}^{NA} D_n = C_K N_{\rm eff}(|\tilde{C}_1|^2 R_0 + |\tilde{B}|^2 R_n) \ , \tag{9}$$

$$I_{\rm lab}^{NA} D_q = C_K N_{\rm eff}(|\tilde{D}_1|^2 R_p + |\tilde{E}|^2 R_q) \ , \tag{10}$$

$$I_{\rm lab}^{NA} D_p = C_K N_{\rm eff}(|\tilde{D}_2|^2 R_q + |\tilde{F}|^2 R_p) \ , \tag{11}$$

where C_K is a kinematic factor, $N_{\rm eff}$ is a distortion factor representing the effective number of neutrons, the terms multiplying the responses are optimal-frame nucleon-nucleon partial cross sections converted to the laboratory frame, and the responses are normalized to the neutron number N. In the following sections we outline the definitions and procedures required to apply these equations.

TABLE III. Cross section (laboratory), polarization, and analyzing power for the ^{40}Ca$(\vec{p},\vec{n})$ reaction at 495 MeV and $\theta_{\rm lab} = 18°$. The uncertainties are from counting statistics only.

ω (MeV)	$\sigma(\omega)$ [mb/(sr 10-MeV)]	A_y	P
160.0	1.3925±0.0038	0.129±0.005	0.158±0.027
150.0	3.3770±0.0059	0.138±0.003	0.189±0.017
140.0	3.9171±0.0063	0.148±0.003	0.210±0.016
130.0	4.4881±0.0068	0.150±0.003	0.212±0.014
120.0	5.1470±0.0072	0.151±0.003	0.187±0.013
110.0	5.7253±0.0076	0.149±0.002	0.185±0.013
100.0	6.1511±0.0079	0.152±0.002	0.165±0.012
90.0	6.4934±0.0082	0.164±0.002	0.159±0.011
80.0	6.5545±0.0082	0.161±0.002	0.165±0.011
70.0	6.3815±0.0081	0.170±0.002	0.169±0.011
60.0	5.8510±0.0078	0.173±0.002	0.141±0.012
50.0	4.8763±0.0071	0.178±0.003	0.178±0.013
40.0	3.5168±0.0060	0.182±0.003	0.173±0.016
30.0	2.1906±0.0048	0.205±0.004	0.178±0.021

A. Polarization observables

Several papers have defined polarization observables appropriate for investigating specific spin channels in inelastic scattering to discrete states [36, 37] and for quasifree scattering with free NN kinematics [6, 7, 10]. In this work we shall use the general relativistic transformation of observables recently outlined by Ichimura and Kawahigashi [38].

Four c.m. frame observables D_i of particular importance can be defined in terms of the laboratory-frame polarization-transfer coefficients D_{ij}. These observables are given by

$$D_0 = \tfrac{1}{4}[1 + D_{N'N} + (D_{S'S} + D_{L'L})\cos(\alpha_1) - (D_{S'L} - D_{L'S})\sin(\alpha_1)] \ , \tag{12}$$

$$D_n = \tfrac{1}{4}[1 + D_{N'N} - (D_{S'S} + D_{L'L})\cos(\alpha_1) + (D_{S'L} - D_{L'S})\sin(\alpha_1)] \ , \tag{13}$$

$$D_q = \tfrac{1}{4}[1 - D_{N'N} + (D_{S'S} - D_{L'L})\cos(\alpha_2) - (D_{S'L} + D_{L'S})\sin(\alpha_2)] \ , \tag{14}$$

$$D_p = \tfrac{1}{4}[1 - D_{N'N} - (D_{S'S} - D_{L'L})\cos(\alpha_2) + (D_{S'L} + D_{L'S})\sin(\alpha_2)] \ , \tag{15}$$

with the constraint

$$D_0 + D_n + D_q + D_p = 1 \ . \tag{16}$$

These observables follow from the original definitions of Blesynski, Blesynski, and Whitten [37], who considered the limits of an infinitely heavy target and small energy loss. The present definitions apply to the general relativistic transformation to the c.m. frame.

The laboratory-frame coordinates (S, N, L) and (S', N', L') were defined in Sec. III. The corresponding c.m. coordinates (q, n, p) are defined as

$$\hat{\mathbf{q}} = \frac{\mathbf{k}_f - \mathbf{k}_i}{|\mathbf{k}_f - \mathbf{k}_i|}, \quad \hat{\mathbf{n}} = \frac{\mathbf{k}_i \times \mathbf{k}_f}{|\mathbf{k}_i \times \mathbf{k}_f|}, \quad \text{and } \hat{\mathbf{p}} = \hat{\mathbf{q}} \times \hat{\mathbf{n}} \ , \tag{17}$$

where k_i and k_f are the initial and final projectile momenta in the NA c.m. frame. The angles α_1 and α_2 are

TABLE IV. Polarization-transfer observables for the ^{2}H$(\vec{p},\vec{n})$ reaction at 495 MeV and $\theta_{\rm lab} = 18°$. The uncertainties are from counting statistics and subtraction systematics.

ω (MeV)	D_{NN}	$D_{S'S}$	$D_{L'L}$	$D_{L'S}$	$D_{S'L}$
100.0	-0.128±0.170	-0.428±0.226	-0.424±0.201	-0.125±0.179	-0.007±0.145
90.0	-0.149±0.109	-0.207±0.109	-0.460±0.117	-0.056±0.109	-0.199±0.101
80.0	0.076±0.060	-0.239±0.064	-0.512±0.064	-0.052±0.064	-0.132±0.056
70.0	-0.021±0.036	-0.199±0.038	-0.453±0.034	-0.034±0.038	-0.083±0.033
60.0	0.006±0.029	-0.211±0.030	-0.466±0.027	-0.029±0.030	-0.111±0.027
50.0	0.043±0.040	-0.294±0.042	-0.514±0.039	-0.047±0.042	-0.144±0.037
40.0	-0.143±0.081	0.060±0.085	-0.360±0.075	-0.172±0.086	-0.088±0.074

TABLE V. Polarization-transfer observables for the $^{12}C(\vec{p},\vec{n})$ reaction at 495 MeV and $\theta_{lab} = 18°$. The uncertainties are from counting statistics only.

ω (MeV)	D_{NN}	$D_{S'S}$	$D_{L'L}$	$D_{L'S}$	$D_{S'L}$
160.0	0.020±0.060	-0.376±0.063	-0.401±0.049	0.159±0.064	-0.060±0.048
150.0	0.071±0.040	-0.292±0.039	-0.443±0.033	0.127±0.040	-0.025±0.032
140.0	0.108±0.036	-0.347±0.036	-0.423±0.030	0.047±0.036	-0.035±0.030
130.0	0.087±0.033	-0.261±0.033	-0.461±0.028	0.061±0.033	-0.053±0.027
120.0	0.076±0.030	-0.326±0.030	-0.431±0.025	0.038±0.030	-0.040±0.025
110.0	0.049±0.027	-0.357±0.027	-0.423±0.023	0.036±0.028	-0.089±0.023
100.0	0.046±0.026	-0.300±0.026	-0.452±0.022	0.058±0.026	-0.080±0.022
90.0	0.096±0.024	-0.338±0.024	-0.463±0.021	0.000±0.025	-0.051±0.021
80.0	0.036±0.024	-0.314±0.024	-0.482±0.021	0.007±0.024	-0.118±0.020
70.0	0.034±0.024	-0.256±0.024	-0.479±0.021	-0.011±0.025	-0.063±0.021
60.0	0.080±0.025	-0.229±0.026	-0.521±0.022	0.016±0.026	-0.054±0.022
50.0	0.045±0.028	-0.213±0.028	-0.514±0.024	0.066±0.029	-0.026±0.024
40.0	0.027±0.032	-0.299±0.032	-0.564±0.028	-0.010±0.033	-0.030±0.028
30.0	0.083±0.032	-0.323±0.032	-0.585±0.028	-0.031±0.033	-0.049±0.027

defined by

$$\alpha_1 = \theta_{c.m.} - \alpha_0 \ , \tag{18}$$

$$\alpha_2 = 2\theta_p - \theta_{c.m.} + \alpha_0, \tag{19}$$

where

$$\cos(\alpha_0) = \cos(\theta_{c.m.})\cos(\theta_{lab}) + \gamma \sin(\theta_{c.m.})\sin(\theta_{lab}) \ . \tag{20}$$

The angle α_0 is related to the relativistic angle Ω used by Ichimura and Kawahigashi [38] by $\alpha_0 = \theta_{c.m.} - \theta_{lab} - \Omega$. Also, $\theta_p = \theta_q - \pi/2$ and $\gamma = E_{lab}/E_{c.m.}$. In the special case of free nucleon-nucleon scattering, for which

$$\begin{aligned} \theta_p &= \tfrac{1}{2}\theta_{c.m.} \ , \\ \alpha_0 &= \theta_{lab} \ , \\ \alpha_1 &= \theta_{c.m.} - \theta_{lab} \ , \\ \alpha_2 &= \theta_{lab} \ , \end{aligned} \tag{21}$$

and

$$\tan(\theta_{lab}) = \frac{D_{S'L} + D_{L'S}}{D_{L'L} - D_{S'S}} \ , \tag{22}$$

the above equations reduce to those employed in previous analyses of quasifree scattering [6, 7, 10], with the identification $D_q^{NN} = S_L$, and $D_p^{NN} = S_T$.

B. Nucleon-nucleon optimal frame

The significance of the c.m. observables D_i can be easily appreciated by their application to free NN scattering. The c.m. nucleon-nucleon charge-exchange scattering amplitude can be expressed in a standard form [39] as

$$M(q) = A + C(\sigma_{0n} + \sigma_{1n}) + B\sigma_{0n}\sigma_{1n} + E\sigma_{0q}\sigma_{1q} + F\sigma_{0p}\sigma_{1p} \ , \tag{23}$$

TABLE VI. Polarization-transfer observables for the $^{40}Ca(\vec{p},\vec{n})$ reaction at 495 MeV and $\theta_{lab} = 18°$. The uncertainties are from counting statistics only.

ω (MeV)	D_{NN}	$D_{S'S}$	$D_{L'L}$	$D_{L'S}$	$D_{S'L}$
160.0	0.070±0.057	-0.245±0.050	-0.467±0.052	0.198±0.051	0.038±0.051
150.0	0.030±0.036	-0.294±0.034	-0.408±0.034	0.097±0.035	-0.031±0.034
140.0	0.037±0.033	-0.254±0.031	-0.404±0.032	0.034±0.032	-0.016±0.031
130.0	0.113±0.031	-0.315±0.029	-0.487±0.029	0.043±0.030	-0.027±0.029
120.0	0.097±0.028	-0.340±0.027	-0.489±0.027	0.108±0.027	-0.064±0.027
110.0	0.061±0.026	-0.359±0.025	-0.454±0.025	0.059±0.025	-0.035±0.025
100.0	0.084±0.025	-0.295±0.024	-0.444±0.024	0.023±0.024	-0.089±0.024
90.0	0.077±0.024	-0.316±0.023	-0.520±0.023	0.058±0.023	-0.043±0.023
80.0	0.079±0.024	-0.251±0.023	-0.468±0.023	-0.011±0.023	-0.055±0.023
70.0	0.080±0.024	-0.223±0.023	-0.511±0.023	0.029±0.023	-0.056±0.023
60.0	0.021±0.025	-0.276±0.024	-0.509±0.024	-0.001±0.024	-0.052±0.024
50.0	0.085±0.028	-0.297±0.026	-0.463±0.027	0.039±0.027	0.002±0.027
40.0	0.123±0.033	-0.231±0.032	-0.477±0.033	-0.004±0.032	-0.032±0.032
30.0	0.063±0.043	-0.246±0.041	-0.537±0.042	0.059±0.042	-0.090±0.042

where σ_0 and σ_1 are the Pauli spin matrices for the projectile and target nucleon projected onto the NN c.m. coordinate axes (q,n,p). In this case the NN c.m. partial cross sections

$$I_0^{NN} = I^{NN} D_0^{NN} = |A|^2 + |C|^2 , \quad (24)$$

$$I_n^{NN} = I^{NN} D_n^{NN} = |B|^2 + |C|^2 , \quad (25)$$

$$I_q^{NN} = I^{NN} D_q^{NN} = |E|^2 , \quad (26)$$

$$I_p^{NN} = I^{NN} D_p^{NN} = |F|^2 , \quad (27)$$

select very simple combinations of amplitudes. Similar combinations appear in Eqs. (8)–(11) for NA quasifree scattering. However, in the NA case the amplitudes are chosen to be those in an "optimal" NN scattering frame that provides the best factorization of the NN t matrix from the nuclear structure transition amplitude. The optimal frame most appropriate for large-energy-loss quasifree scattering has been discussed in detail by Gurvitz [40] and Zhu *et al.* [41], briefly by Smith [33, 35], and recently in detail by Ichimura and Kawahigashi [38]. The choice of optimal frame introduces some kinematic factors and complications owing to frame rotation. We follow the definitions in Ref. [38] and summarize the main points below.

The t matrix T^η in the optimal frame is related to the scattering amplitude of Eq. (23) by the transformation

$$T^\eta = J(\eta)\mathcal{R}(\eta)\left(-\frac{4\pi}{E(k)}M^{NN}\right) , \quad (28)$$

where $J(\eta)$ is the Möller factor, $\mathcal{R}(\eta)$ is the transformation matrix defined in Ref. [38], and $E(k)$ is the projectile energy in the NN c.m. frame. In the optimal frame T^η has the form

$$T^\eta = T_0^\eta + T_n^\eta \sigma_{0n} + T_q^\eta \sigma_{0q} + T_p^\eta \sigma_{0p} , \quad (29)$$

with components

$$T_0^\eta = A^\eta + C_2^\eta \sigma_{in} , \quad (30)$$

$$T_n^\eta = B^\eta \sigma_{in} + C_1^\eta , \quad (31)$$

$$T_q^\eta = E^\eta \sigma_{iq} + D_1^\eta \sigma_{ip} , \quad (32)$$

$$T_q^\eta = D_2^\eta \sigma_{iq} + F^\eta \sigma_{ip} , \quad (33)$$

where the coordinates (q,n,p) are defined in terms of the NA c.m. momenta $\mathbf{k}_i$ and $\mathbf{k}_f$. With this t matrix, the NA c.m. partial cross sections are obtained from

$$I_{\text{c.m.}}^{NA} D_i = 2K^{NA} \text{Tr}'[T_i^\eta T_i^{\eta\dagger}] . \quad (34)$$

Conversion of the cross sections to the laboratory frame and factorization of the projectile distorted waves from the nuclear transition amplitude then leads to Eqs. (8)–(11). This factorized impulse approximation derivation ignores interference between the different spin channels.

The kinematic factor C_K that appears in Eqs. (8)–(11) is given by

$$C_K = \frac{1}{2}\left(\frac{\sigma_{\text{c.m.}}}{\sigma_{\text{lab}}}\right)^{-1}_{NA}\left(\frac{\sigma_{\text{c.m.}}}{\sigma_{\text{lab}}}\right)_{NN} J(\eta)^2 \frac{K^{NA}}{K^{NN}} , \quad (35)$$

where

$$K = \frac{E_i E_f}{(2\pi)^2}\frac{k_f}{k_i}\frac{1}{2(2J_i+1)} , \quad (36)$$

and E_i and E_f are the reduced energies in the NA c.m. frame. For NN scattering,

$$4K^{NN} = \left[\frac{E(k)}{4\pi}\right]^2 . \quad (37)$$

The factor C_K has a value of approximately 1 (for $J_i = 0$) and varies slowly with energy loss. For $^{12}\text{C}(p,n)$, it varies from $C_K = 1.012$ to 0.772 over the range $\omega =$ 30–160 MeV.

The η-frame NN amplitudes are calculated at an effective laboratory bombarding energy $T_{\text{lab}}^{\text{eff}}$ and scattering angle $\theta_{\text{lab}}^{\text{eff}}$ determined by the invariant energy s_{eff} in the optimal frame [38] and the invariant momentum transfer $t_{\text{eff}} = \omega_{\text{lab}}^2 - q_{\text{lab}}^2$ [42, 33]. Some typical values for ^{12}C are

ω (MeV)	30	60	160
$T_{\text{lab}}^{\text{eff}}$ (MeV)	524	492	340
$\theta_{\text{lab}}^{\text{eff}}$ (deg)	17.5	18.0	23.4

which show that the effective laboratory bombarding energy varies by nearly 200 MeV over the range of the present data. This variation can have important consequences if the amplitudes are strongly energy dependent, as is the case for the isoscalar amplitudes present in the (p,p') reaction [9]. The squared isovector amplitudes obtained from the transformation $M' = R(\eta)M$ are displayed in Fig. 7. As indicated in Ref. [38], the mixing be-

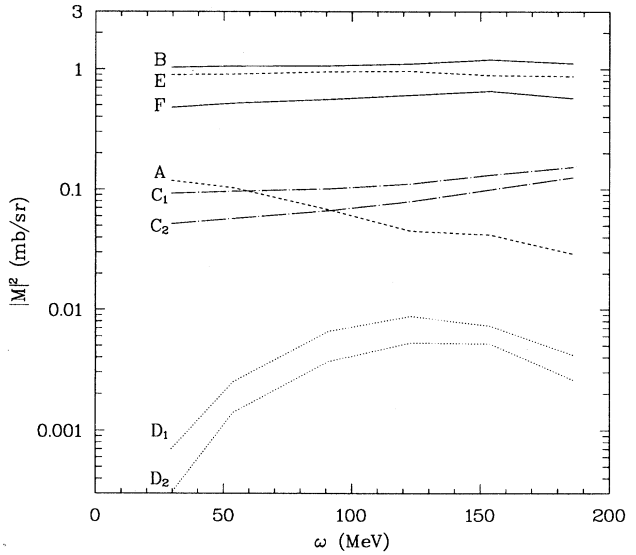

FIG. 7. Squared np amplitudes $M' = R(\eta)M$ [see Eq. (28)] from the Bugg-Bryan [28] phase-shift solution. The amplitudes are derived according to optimal-frame kinematics. In descending order of magnitude (for $\omega = 30$ MeV) they are: B, E, F, A, C_1, C_2, D_1, and D_2. The relative energy dependence of A, C_1, and C_2 has a significant effect in the extraction of the R_0 and R_n responses.

tween R_q and R_p induced by the optimal-frame factorization is negligible because the amplitudes D_1^η and D_2^η are very small. For the present case, $|D_1^\eta/E^\eta|^2 \approx |D_2^\eta/F^\eta|^2 \lesssim 0.01$. The amplitudes A^η, C_1^η, and C_2^η are also small but not negligible and must be properly accounted for in extracting the responses R_0 and R_n.

If the D_1^η and D_2^η amplitudes are neglected, then Eqs. (10) and (11) can be rewritten as

$$I_{\rm lab}^{NA} D_q^{NA} = C_K I_{\rm lab}^{NN} D_q^{NN} N_{\rm eff} R_q \ , \tag{38}$$

$$I_{\rm lab}^{NA} D_p^{NA} = C_K I_{\rm lab}^{NN} D_p^{NN} N_{\rm eff} R_p \ , \tag{39}$$

where Eqs. (26) and (27) have been used to substitute NN observables for the $|E|^2$ and $|F|^2$ amplitudes. The cross section and polarization-transfer coefficients for ^{2}H(p,n) can in turn be used as good representations of these free NN observables. This is the strategy employed in previous analyses [6, 7, 18]. This method will not account for any energy dependence of the observables with respect to the effective energy $T_{\rm lab}^{\rm eff}$ away from the quasifree point. However, the ^{2}H data can provide a valuable check on the accuracy of the NN amplitudes obtained from phase-shift solutions. The c.m. polarization observables [Eqs. (12)–(15)] for ^{2}H are plotted in Fig. 8 along with free NN values derived from the FA91 phase-shift solution of Arndt [27] and a phase-shift solution of Bugg and Bryan parametrized by Arndt [28]. The phase-shift values are computed according to the optimal-frame kinematics. The experimental values have been computed for a target mass of $A = 2$, but there is negligible difference if $A = 1$ (free kinematics) is assumed. The two solutions do comparably well for the observables D_0 and D_n, but the solution of Bugg and Bryan [28] does better for D_q and D_p, which are directly related to the R_q and R_p responses. The difference between the two phase-shift solutions can be further assessed by looking at the ratio $D_q/D_p = |E/F|^2$. This ratio is shown in Fig. 9. The ratio obtained from the Bugg-Bryan solution [28] (solid line) is very close to the experimental ratio, while the values from Arndt [27] (dashed line) are too high. A more recent phase-shift solution from Bugg and Bryan [43] gives a larger value ($|E/F|^2 = 2.08$), indicating that the free amplitudes may not yet be well constrained in this kinematic region. Because of their closer agreement with the ^{2}H(p,n) data, we shall employ the earlier Bugg-Bryan amplitudes to extract the nuclear responses and response ratios. This provides a convenient way to account for the energy dependence introduced by the optimal-frame factorization without extensive renormalization of the amplitudes.

C. Distortion factor

The distortion factor $N_{\rm eff}$ acts as an overall attenuation factor and is represented in the form of an effective number of target nucleons (in this case neutrons). In the present treatment of $N_{\rm eff}$, we ignore the effects of spin-dependent distortions, which have been estimated to be small [34, 44]. The single-scattering eikonal approxima-

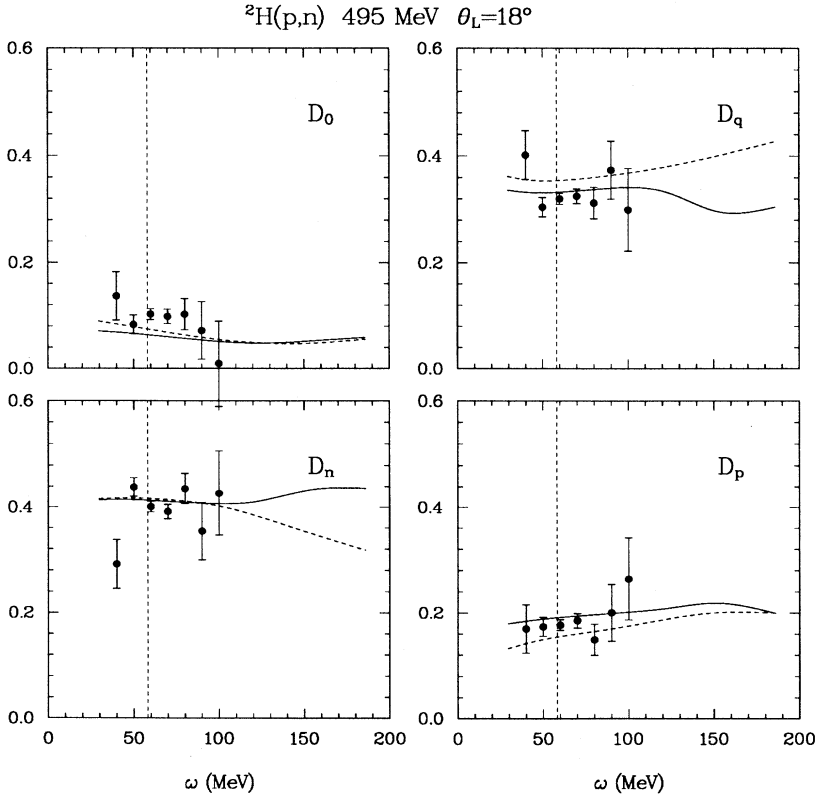

FIG. 8. Polarization-transfer observables for ^{2}H(p,n) compared to optimal-frame free np values. The solid horizontal lines represent the optimal-frame np values from the phase-shift solution of Bugg and Bryan [28]. The dashed horizontal lines are from the FA91 phase-shift solution of Arndt [27]. The dashed vertical lines mark the energy loss for free np scattering.

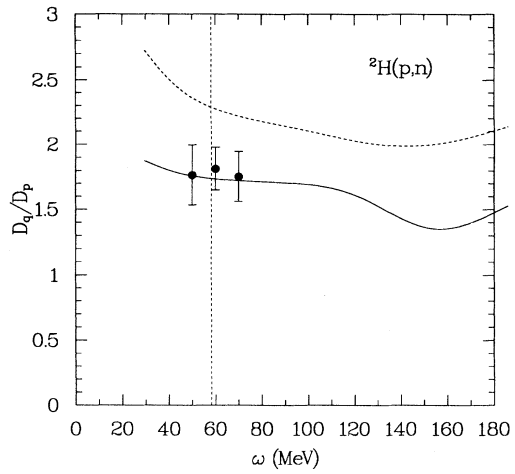

FIG. 9. Ratio of observables D_q/D_p for $^2\mathrm{H}(p,n)$. The solid horizontal line represents the optimal-frame np ratio from the phase-shift solution of Bugg and Bryan [28]. The dashed horizontal line is from the FA91 phase-shift solution of Arndt [27]. The dashed vertical line marks the energy loss for free np scattering.

tion to N_{eff} is given by

$$N_{\mathrm{eff}} = \frac{N}{A}\int_0^\infty b\,db\,n(b)\exp[-n(b)\tilde{\sigma}_{NN}]\,, \tag{40}$$

where $\tilde{\sigma}_{NN}$ is the total NN cross section in the nuclear medium and

$$n(b) = \int_{-\infty}^{+\infty} dz\,\rho_A[(z^2+b^2)^{1/2}]\,. \tag{41}$$

The factor N/A is required to obtain the effective number of neutrons. The nuclear density is described by shape parameters taken from Ref. [45]. The total NN cross section is calculated following the method of Smith and Bozoian [35], who obtain the in-medium cross section from the imaginary optical potential according to

$$\tilde{\sigma}_{NN}(E) = \frac{2m}{k}J_W/A\,, \tag{42}$$

with the parametrization $J_W/A = 0.6E$ MeV fm^3. This gives a total cross section of $\tilde{\sigma}_{NN} = 21$–26 mb over the energy range 300–500 MeV. This in-medium cross section is somewhat smaller than the free NN total cross section $\sigma_{NN} = \frac{1}{2}(\sigma_{np}+\sigma_{pp})$, which varies from 29.5 mb to 32 mb over the same energy range [27]. The energy dependence of the in-medium NN cross section and the large energy loss involved in the quasifree reaction will introduce some energy dependence into the calculated values of N_{eff}. We account for this energy dependence by using an average value $\tilde{N}_{\mathrm{eff}} = \frac{1}{2}[N_{\mathrm{eff}}(E_p)+N_{\mathrm{eff}}(E_n)]$ for each outgoing neutron energy. Over the neutron energy range 300–500 MeV, this gives values of $\tilde{N}_{\mathrm{eff}} = 2.40$–$2.21$ for ^{12}C and $\tilde{N}_{\mathrm{eff}} = 5.03$–$4.48$ for ^{40}Ca. The values obtained by using the larger free NN cross section rather than the in-medium cross section are about 20% smaller. Some authors have used NN cross sections as large as $\sigma_{NN} = 40$ mb in calculating the eikonal distortion factor [11, 32]. This inexplicably large value results in effective neutron numbers about 40% smaller than those obtained from the in-medium cross sections.

D. Response functions

The response functions R_j derived from Eq. (34) and used in Eqs. (8)–(11) are defined by [38]

$$R_j = \frac{1}{N}\sum_n \left|\left\langle \Psi_{n,-\mathbf{k}_f}\left|\sum_{i=1}^{N}(\sigma_j)_i e^{-i\mathbf{q}\cdot\mathbf{r}_i}\right|\Psi_{0,-\mathbf{k}_i}\right\rangle\right|^2 \delta(\omega-(E_A^n-E_A^0))\,, \tag{43}$$

with $j = 0, n, p, q$, and are normalized such that in the limit of no Pauli blocking

$$\int R(\omega)\,d\omega \to 1 \qquad \text{for } q\to\infty\,. \tag{44}$$

This normalization differs by a factor of $2/N$ from that used by Ichimura and Kawahigashi [38], and is defined so as to give the response per neutron. This normalization (per neutron) is a consequence of expressing the distortion factor in terms of an effective neutron number.

The responses extracted from the $\mathrm{C}(p,n)$ and $\mathrm{Ca}(p,n)$ data according to Eqs. (8)–(11) are displayed in Fig. 10. The results for C and Ca are very similar. This is not surprising owing to the great similarity in the polarization transfer observables. The close agreement in magnitude between the C and Ca results also indicates that the calculated kinematic and distortion factors have properly accounted for the target mass dependence. The systematic experimental uncertainty in the magnitude of the responses is about 6% from the cross section normalization and about 2% from the polarization observables D_i.

Apart from experimental uncertainties, there are several potential sources of systematic error in the absolute magnitude of the separated responses: model dependence associated with calculation of the distortion factors, uncertainty introduced by the choice of phase-shift solution used to generate the NN amplitudes, and multiple-scattering effects.

The uncertainty associated with the NN amplitudes is largest for the R_0 and R_n responses, which are mixed together by small amplitudes, one of which (A^η) has considerable energy dependence. Even for the R_q and R_p responses, the uncertainty can be significant, however. For example, at large energy loss (and therefore smaller $T_{\mathrm{lab}}^{\mathrm{eff}}$) differences as large as 50% exist in the squared

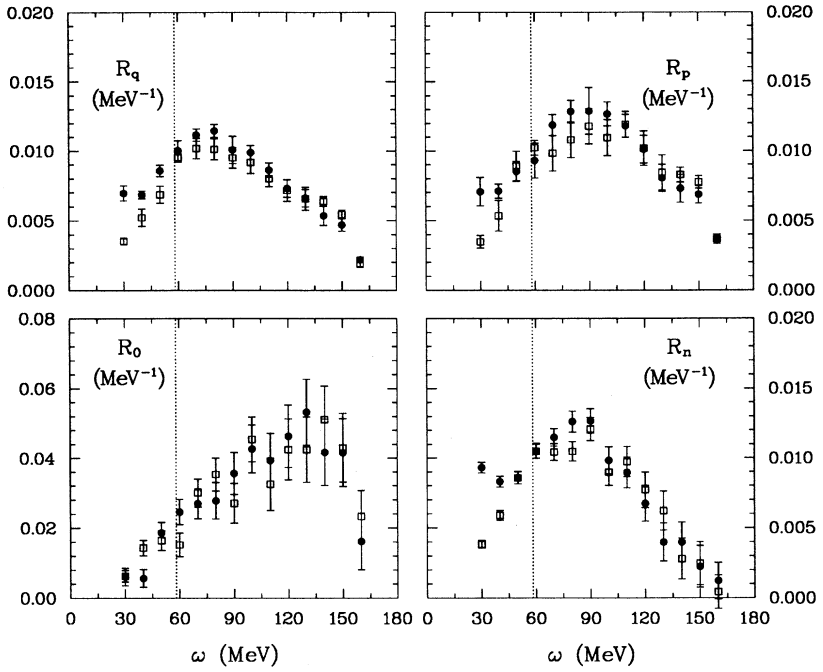

FIG. 10. The four responses R_0, R_q, R_n, and R_p for C (solid circles) and Ca (open squares). The responses are extracted from the data according to Eqs. (8)–(11) with optimal-frame np amplitudes from the phase-shift solution of Bugg and Bryan [28]. Dotted vertical lines mark the energy loss for free np scattering.

amplitudes $|E|^2$ and $|F|^2$ obtained from the Arndt and Bugg-Bryan phase shifts. To some extent this uncertainty associated with the amplitudes can be minimized by normalizing to the ^{2}H(p,n) results. This works well only near the peak of the ^{2}H(p,n) distribution, however.

Much of the uncertainty associated with distortion effects can be removed by looking at ratios of responses. Two ratios of interest are formed from the longitudinal spin response R_q and the two transverse spin responses R_n and R_p. These ratios are displayed in Fig. 11. The ratio R_q/R_p has a particularly simple form in terms of polarization observables and NN amplitudes,

$$\frac{R_q}{R_p} = \frac{D_q/D_p}{|E/F|^2} \,. \tag{45}$$

Furthermore, near the quasifree point, the amplitude ratio $|E/F|^2$ can be replaced by the ratio $(D_q/D_p)_{^2\mathrm{H}}$ for ^{2}H(p,n), as in Eqs. (38) and (39). This then gives

$$\frac{R_q}{R_p} = \frac{D_q/D_p}{(D_q/D_p)_{^2\mathrm{H}}} \,, \tag{46}$$

where now the response ratio is obtained entirely in terms of experimentally measured polarization observables. This latter ratio, however, has the disadvantage that it does not account for the energy dependence of the NN amplitudes, as shown in Fig. 9. This energy dependence amounts to a change of about 30% in $|E/F|^2$ over the range of the present data. Use of the Arndt FA91 phase shifts [27], normalized to the ^{2}H data, would introduce differences in this ratio of about ±10% compared to the values extracted using the Bugg-Bryan phase shifts [28].

The present application of Eqs. (8)–(11) neglects the contribution of double-scattering and higher-order processes to the inclusive cross section. Calculations by Smith and Wallace [34] and Esbensen and Bertsch [46] indicate that the multiple-scattering contributions to the cross section are on the order of 10% for (p,p') quasifree scattering, with corresponding small effects on the spin observables [34]. Multiple-scattering contributions are expected to be larger in charge-exchange reactions, how-

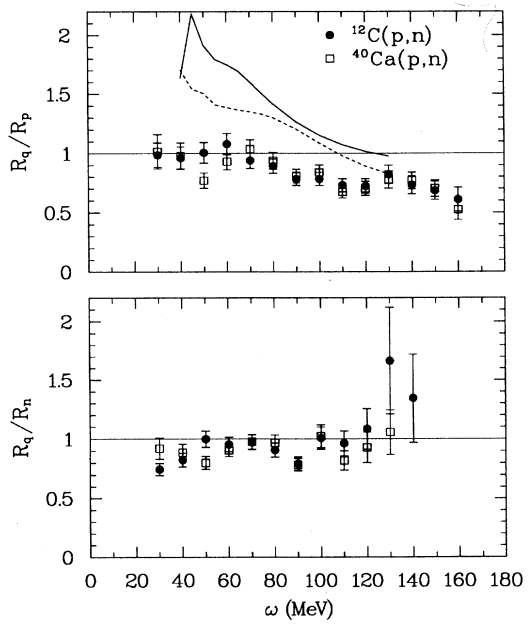

FIG. 11. Ratio of spin responses R_q/R_p and R_q/R_n for C (solid circles) and Ca (open squares). The ratio is computed according to Eq. (45) with optimal-frame np amplitudes from the phase-shift solution of Bugg and Bryan [28]. The ratios of RPA responses [17] for C (solid) and Ca (dashed) are plotted in the top panel.

ever [33]. A recent analysis of 800 MeV quasifree (p,n) data by Prout [47] points to conditions under which a substantial fraction of the cross section in the quasifree region may be attributed to double scattering. The double-scattering contribution becomes more important with increasing scattering angle and target mass number, and may contribute as much as 30% of the cross section at the peak of the quasifree distribution for Pb(p,n) at 800 MeV and $q > 2$ fm^{-1}. For the present case, the estimated double-scattering contribution is on the order of 10–15 %. We shall make use of the single-scattering assumption in the present analysis, but the contribution of higher-order terms must be considered more carefully in drawing conclusions from future data at larger momentum transfers.

V. COMPARISON TO ELECTRON SCATTERING

The transverse spin responses for ^{12}C(e,e') and ^{40}Ca(e,e') have been determined at several momentum transfers. The measurements that most closely match the present experiment are those of Barreau *et al.* [2] for ^{12}C at $q = 1.77$ fm^{-1} (350 MeV/c) and those of Deady *et al.* [3, 4] for ^{40}Ca at $q = 1.67$ fm^{-1} (330 MeV/c) and 1.88 fm^{-1} (370 MeV/c). Deady *et al.* report their data according to the convention of Eq. (6), while Barreau *et al.* report the quantity $(4\pi/M_T)S_T$.

The transverse structure function in Eq. (6) corresponds to magnetic scattering from Z protons and N neutrons. This target dependence can be accounted for by extracting a normalized (per nucleon) response R_T according to [1, 48]

$$\frac{4\pi}{M_T}S_T = \frac{q^2}{e^2}(Z\mu_p^2 + N\mu_n^2)G_M^2 R_T \,, \tag{47}$$

where $\mu_p = 2.79\mu_N$, $\mu_n = -1.91\mu_N$, and G_M is the nucleon magnetic form factor,

$$G_M(q_\mu^2) = [1 + q_\mu^2/(0.71\,\mathrm{GeV}^2)]^{-2} \,, \tag{48}$$

with $q_\mu^2 = \mathbf{q}^2 - \omega^2$. This R_T response can now be compared directly to the R_n and R_p $(\vec{p},\vec{n})$ responses. This comparison is made in Fig. 12. The electron scattering data in this figure have been normalized by an additional factor $r_{SV} = 0.71$ for ^{12}C and $r_{SV} = 0.83$ for ^{40}Ca. The significance of this factor is discussed below. The normalized (e,e') and (p,n) responses agree well in shape and peak location. The (p,n) transverse spin responses peak at about $\omega = 90$ MeV ($q_{\mathrm{c.m.}} = 1.72$ fm^{-1}), or about 32 MeV above the energy loss for free np scattering ($\omega = 58$ MeV).

Reaction theory indicates that the responses obtained from (p,n) and (p,p') measurements are surface responses rather than the volume response probed by electron scattering. In the eikonal calculations outlined in the preceding section, the quantity dN_{eff}/db gives the reaction contribution as a function of impact parameter [32]. In this model, most of the single-scattering cross section corresponds to interactions in the nuclear surface where the density is only about 1/4–1/3 of the core density.

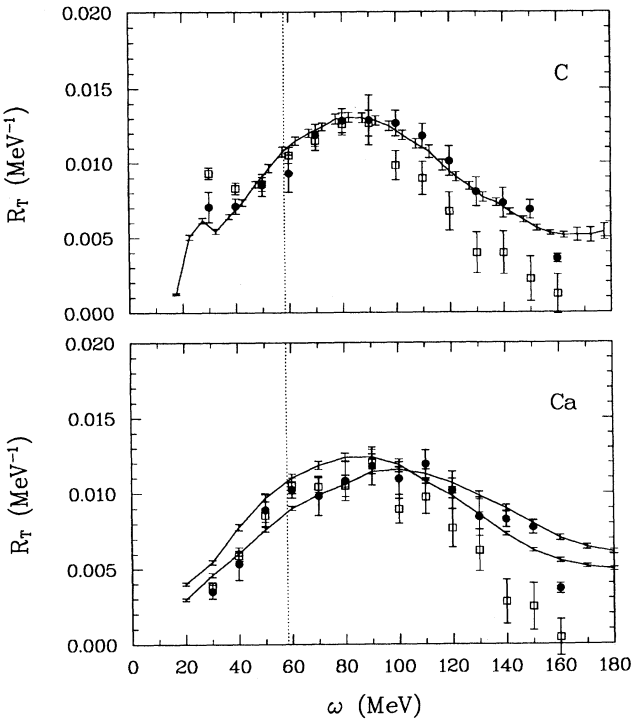

FIG. 12. The transverse spin responses R_p (solid circles) and R_n (open squares) from ^{12}C(p,n) and ^{40}Ca(p,n) at $q_{\mathrm{c.m.}} = 1.72$ fm^{-1} compared to the transverse responses from ^{12}C(e,e') at $q = 1.77$ fm^{-1} [2] and ^{40}Ca(e,e') at $q = 1.67$ and 1.88 fm^{-1} [4]. Solid lines connect the (e,e') values, which are plotted as error bars without symbols. Dotted vertical lines mark the energy loss for free np scattering. The (e,e') responses have been normalized by factors of $r_{SV} = 0.71$ and 0.83 for ^{12}C and ^{40}Ca, respectively.

The surface localization of the (p,n) reaction might produce a weakening of collective effects, a distortion of the shape of the response or a shift in the peak position, or a mixing between the longitudinal and transverse channels [48–52]. From the present comparison, the main effect seems to be simply a minimal overall scaling of the response with little distortion in shape or shift in position. The difference between the experimental (p,n) surface response and the (e,e') volume response may therefore be summed up in the simple scaling factor $r_{SV} \simeq 0.75$. The significance of this factor is unclear. Collective effects in the transverse channel are expected to quench R_T with respect to the free response, so a decrease in collectivity due to surface effects should produce a value $r_{SV} > 1$. Experimental and distortion uncertainties will also contribute to this factor, as well as multiple-scattering contributions to the (p,n) cross section and neglect of the small isoscalar contribution to the (e,e') cross section. Another contribution may be the inexact correspondence between the transverse operators for the electron and nucleon probes.

In spite of the many factors that can potentially al-

ter the relationship between the (e,e') and (p,n) transverse responses, the similarity in shape and magnitude is remarkable. This close agreement therefore supports a straightforward interpretation of the (p,n) responses. The relevance of our present results with respect to expected collective effects is discussed in the next section.

VI. INTERPRETATION OF THE RESPONSES

The magnitude and centroid of the isovector spin responses should reflect the gross properties of the underlying particle-hole interaction. The standard form for this interaction is generally taken to be [1]

$$V(q,\omega) = \left(\frac{f^2}{m_\pi^2}\right)\left\{\left[g' + \frac{q^2}{\omega^2 - (q^2+m_\pi^2)}\Gamma_\pi^2(q,\omega)\right](\boldsymbol{\sigma}_1\cdot\hat{\mathbf{q}})(\boldsymbol{\sigma}_2\cdot\hat{\mathbf{q}}) + \left[g' + C_\rho\frac{q^2}{\omega^2 - (q^2+m_\rho^2)}\Gamma_\rho^2(q)\right](\boldsymbol{\sigma}_1\times\hat{\mathbf{q}})\cdot(\boldsymbol{\sigma}_2\times\hat{\mathbf{q}})\right\}\boldsymbol{\tau}_1\cdot\boldsymbol{\tau}_2, \quad (49)$$

where m_π and m_ρ are the pion and rho masses, respectively, ω is the energy transfer, C_ρ is the ratio of the ρ and π coupling, f^2 is the πNN coupling constant, and Γ_π and Γ_ρ are the vertex (monopole) form factors of the π and ρ, respectively. A contact term governed by the Landau-Migdal parameter g' takes into account the short-range repulsive nature of the interaction. The magnitude of this term also determines the magnitude of the interaction at nonzero momentum transfer and energy loss. For a nominal value of $g' = 0.6$, the longitudinal interaction becomes moderately attractive for $q \gtrsim 1$ fm^{-1} while the transverse interaction remains repulsive.

In nuclear matter calculations [1], the attractive interaction in the longitudinal channel leads to an enhancement and softening (shift toward lower energy loss) of the collective response. In the transverse channel, the response should be quenched and hardened (shifted toward higher energy loss). In a real nucleus probed by nucleons, distortions and the lower density in the surface region sampled by the probing reaction can reduce the size of the expected collective effects. However, most calculations that attempt to account for these effects still retain a significant signature of the enhancement of the longitudinal response relative to the transverse response [11, 12, 17].

The ratios of responses presented in Fig. 11 show no evidence for an enhancement of the longitudinal response relative to the transverse response(s). To within the experimental bin uncertainties of about ± 0.07 (statistical) and ± 0.03 (systematic), the ratios R_q/R_p and R_q/R_n are consistent with unity or smaller. Furthermore, as is evident in Fig. 10, the longitudinal response R_q is not softened with respect to free scattering, but instead is hardened by approximately 20 MeV. This shift toward higher energy loss is comparable to the 30 MeV shift present in the transverse response. This comparison therefore suggests that the residual particle-hole interaction in the longitudinal channel is not attractive and may in fact be similar to the repulsive transverse interaction at this momentum transfer. Measurements of quasifree peak positions for (p,n) reactions over the momentum transfer range $q = 1$–3.5 fm^{-1} show an almost constant shift of about 25 MeV toward higher energy loss with respect to free scattering [47]. It therefore seems that the relative characteristics of the longitudinal and transverse interactions do not change substantially over this momentum transfer range. This implies that the standard form of the particle-hole interaction [Eq. (49)] requires substantial modification.

The implications of the present data can be further emphasized by comparison to the RPA responses. In Figs. 13 and 14, we show the experimental longitudinal (R_q) and transverse (R_p,R_n) responses for C and Ca compared to RPA responses ($g' = 0.6$) provided by Ichimura [17]. The dashed lines in these figures represent the free response (no RPA correlations), while the solid lines show

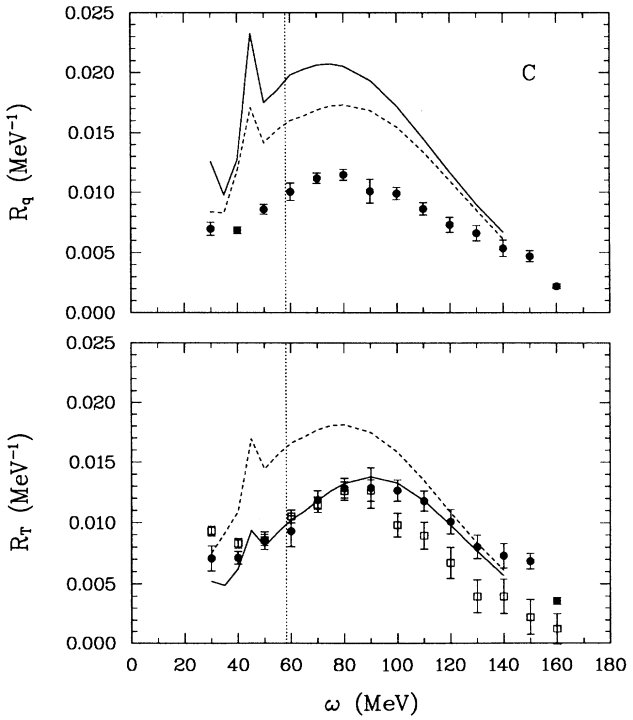

FIG. 13. Longitudinal and transverse spin responses for ^{12}C(p,n) compared to RPA responses from Ichimura [17]. In the bottom panel the open squares represent the R_n response, the solid circles represent the R_p response. Dashed lines show the free response with no RPA correlations. Solid lines are the RPA responses for $g' = 0.6$. Dotted vertical lines mark the energy loss for free np scattering.

how the responses change when the residual particle-hole interaction is turned on. In the case of the transverse response, the agreement with the data is surprisingly good. In the longitudinal channel, the RPA response shows the expected enhancement and softening—quite unlike the experimental response, which is quenched and hardened. The differences are further emphasized in the ratios $(R_q/R_p)_{\mathrm{RPA}}$, which are plotted for C (solid line) and Ca (dashed line) in Fig. 11.

One potential complication that must be considered in the interpretation of the data is the alteration of the NN amplitudes in the nuclear medium. If the NN amplitudes contained in Eqs. (8)–(11) are different from the free amplitudes, then neither the phase-shift solutions nor the $^2\mathrm{H}(p,n)$ data will be sufficient for determining the response functions. Horowitz, Murdock, and Iqbal [42, 44] have used a Fermi-gas model of the quasifree response to calculate how spin observables will be affected by relativistic dynamics in the nuclear medium. Their model correctly predicts the quenching of the polarization P observed in quasifree (p,p') reactions, although it is not so successful for other polarization observables. However, regardless of whether the details of this particular model are correct, medium modifications should manifest themselves by causing the NA polarization observables to differ from the free NN observables. The four c.m. polarization observables for C and Ca are compared to the $^2\mathrm{H}$ results in Fig. 15. Here we have plotted values for $^2\mathrm{H}(p,n)$ for the four bins with highest statistics. Also plotted are values from the two optimal-frame phase-shift solutions. It is immediately evident that the results for the three targets are virtually identical. Given

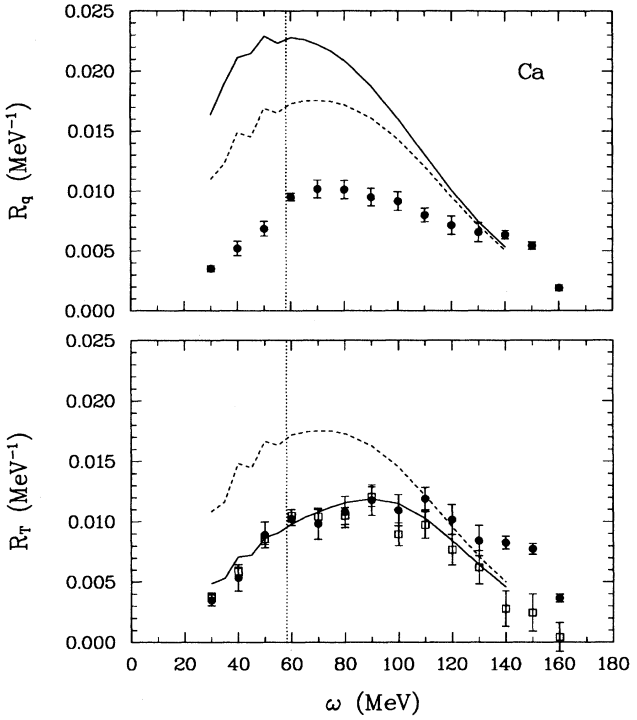

FIG. 14. Longitudinal and transverse spin responses for $^{40}\mathrm{Ca}(p,n)$ compared to RPA responses from Ichimura [17]. In the bottom panel the open squares represent the R_n response, the solid circles represent the R_p response. Dashed lines show the free response with no RPA correlations. Solid lines are the RPA responses for $g' = 0.6$. Dotted vertical lines mark the energy loss for free np scattering.

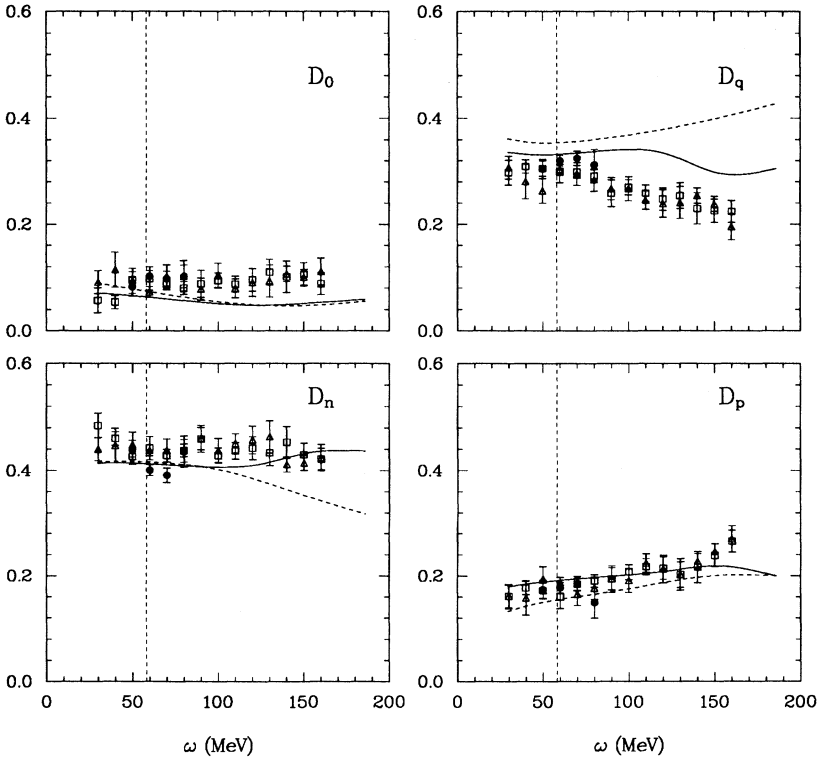

FIG. 15. Polarization observables for $^2\mathrm{H}$ (solid circles) and $^{12}\mathrm{C}$ (open squares) compared to observables for $^{40}\mathrm{Ca}$ (triangles). The solid horizontal line represents the optimal-frame np ratio from the phase-shift solution of Bugg and Bryan [28]. The dashed horizontal line is from the FA91 phase-shift solution of Arndt [27].

the varied collection of additional effects that can also alter the polarization observables, such as collectivity in the nuclear response, distortions, and multiple scattering, it is noteworthy and extremely surprising that the data show little obvious evidence for *any* of them. Experimental signatures for these various effects will have to be sought either at different momentum transfers or at energy transfers away from the quasifree point. In this regard, additional benchmark measurements on ^{2}H that span the effective energy range of the optimal-frame amplitudes will be important.

VII. SUMMARY

The ratios of spin responses determined by the (p,n) reaction essentially confirm the conclusions arrived at from previous studies of (p,p') quasifree scattering: *there is no evidence for an enhancement of the longitudinal response relative to the transverse response at a momentum transfer where this enhancement should be largest.* Because the (p,n) reaction directly probes the isovector spin response, which contributes only a small part of the cross section in the (p,p') reaction, the present results put this conclusion on a much firmer basis. Insight into this problem is provided by information not previously available: a separation of the isovector longitudinal and transverse spin responses in absolute terms. The transverse responses R_n and R_p determined here compare well in shape and magnitude to the transverse response measured in deep inelastic electron scattering. This good agreement therefore suggests a straightforward interpretation of the longitudinal response, which represents new information never before available.

The ratio of isovector spin-longitudinal and spin-transverse responses derived from our analysis of the present data is approximately unity. From this we conclude that the effective particle-hole interaction must be very similar in both channels. The separated transverse responses agree well with both electron scattering results and with RPA calculations incorporating the standard form of the ρ-exchange transverse interaction. From this it is possible to conclude that the interaction in the longitudinal channel is very different from the standard π-exchange form normally assumed. Brown and Rho have proposed [53] a rescaling of the vector meson field that could provide an almost complete cancellation of the attractive pion force by the rho tensor force, leading to a predicted ratio of R_q/R_p close to unity. Additional measurements of the type described in this report will be essential to establish the momentum dependence of these effects, which is expected to be quite different in the Brown and Rho model as compared to the standard picture of the residual interaction.

The present analysis employs a factorized single-scattering reaction model that lends itself to easy interpretation and also provides an estimate of ambiguities associated with distortion effects and the fundamental free np scattering amplitudes. These ambiguities can affect both the magnitude and shape of the extracted longitudinal and transverse responses. Additional measurements of ^{2}H(p,n) quasifree scattering at energies and momentum transfers that constrain the free np amplitudes and remove the inconsistencies between present NN phase-shift solutions would therefore be highly desirable. Careful consideration of multiple-scattering effects will also be necessary. Multiple-scattering contributions to the inclusive cross section are expected to be more important for (p,n) reactions than for (p,p'), and these contributions may have polarization signatures much different from the single-scattering process. It is important, therefore, to analyze these and future data in a model that includes multiple-scattering, distortion, and finite nuclear medium effects in the most realistic and sophisticated manner possible.

ACKNOWLEDGMENTS

We wish to acknowledge extremely helpful conversations and correspondence with Professor M. Ichimura. We are also grateful for many useful discussions with C. Gaarde, Thomas Sams, and J. Shepard. This work was supported by the National Science Foundation and the U.S. Department of Energy.

[1] W.M. Alberico, M. Ericson, and A. Molinari, Nucl. Phys. **A379**, 429 (1982); Ann. Phys. (N.Y.) **131**, 451 (1984).

[2] P. Barreau, M. Bernheim, J. Duclos, J.M. Finn, Z. Meziani, J. Morgenstern, J. Mougey, D. Royer, B. Saghai, D. Tarnowski, S. Turck-Chieze, M. Brussel, G.P. Capitani, E. De Sanctis, S. Frullani, F. Garibaldi, D.B. Isabelle, E. Jans, I. Sick, and P.D. Zimmerman, Nucl. Phys. **A402**, 515 (1983); P. Barreau *et al.*, Note CEA N-2334.

[3] M. Deady, C.F. Williamson, J. Wong, P.D. Zimmerman, C. Blatchley, J.M. Finn, J. LeRose, P. Sioshansi, R. Altemus, J.S. McCarthy, and R.R. Whitney, Phys. Rev. C **28**, 631 (1983).

[4] M. Deady, C.F. Williamson, P.D. Zimmerman, R. Altemus, and R.R. Whitney, Phys. Rev. C **33**, 1897 (1986).

[5] Z.E. Meziani, P. Barreau, M. Bernheim, J. Morgenstern, S. Turck-Chieze, R. Altemus, J. McCarthy, L.J. Orphanos, R.R. Whitney, G.P. Capitani, E. De Sanctis, S. Frullani, and F. Garibaldi, Phys. Rev. Lett. **54**, 1233 (1985).

[6] T.A. Carey, K.W. Jones, J.B. McClelland, J.M. Moss, L.B. Rees, N. Tanaka, and A.D. Bacher, Phys. Rev. Lett. **53**, 144 (1984).

[7] L.B. Rees, J.M. Moss, T.A. Carey, K.W. Jones, J.B. McClelland, N. Tanaka, A.D. Bacher, and H. Esbensen, Phys. Rev. C **34**, 627 (1986).

[8] R. Fergerson, J. McGill, C. Glashausser, K. Jones, S. Nanda, Sun Zuxun, M. Barlett, G. Hoffmann, J. Marshall, and J. McClelland, Phys. Rev. C **38**, 2193 (1988).

[9] O. Häusser, R. Abegg, R.G. Jeppesen, R. Sawafta, A. Celler, A. Green, R.L. Helmer, R. Henderson, K. Hicks, K.P. Jackson, J. Mildenberger, C.A. Miller, M.C. Vetterli, S. Yen, M.J. Iqbal, and R.D. Smith, Phys. Rev.

Lett. **61**, 822 (1988).
[10] C. Chan, T.E. Drake, R. Abegg, D. Frekers, O. Häusser, K. Hicks, D.A. Hutcheon, L. Lee, C.A. Miller, R. Schubank, and S. Yen, Nucl. Phys. **A510**, 713 (1990).
[11] W.M. Alberico, A. De Pace, M. Ericson, Mikkel Johnson, and A. Molinari, Phys. Rev. C **38**, 109 (1988).
[12] M. Ichimura, K. Kawahigashi, T.S. Jørgensen, and C. Gaarde, Phys. Rev. C **39**, 1446 (1989).
[13] D.V. Bugg and C. Wilkin, Nucl. Phys. **A467**, 565 (1987).
[14] C. Wilkin and D.V. Bugg, Phys. Lett. **154B**, 243 (1985).
[15] C. Ellegaard, C. Gaarde, T.S. Jørgensen, J.S. Larsen, C. Goodman, I. Bergqvist, A. Brockstedt, P. Ekström, M. Bedjidian, D. Contardo, J.Y. Grossiord, A. Guichard, D. Bachelier, J.L. Boyard, T. Hennino, J.C. Jourdain, M. Roy-Stephan, P. Radvanyi, and J. Tinsley, Phys. Rev. Lett. **59**, 974 (1987).
[16] Thomas Sams, Ph.D. thesis, Niels Bohr Institute, 1990; in *Proceedings of the International Conference on Spin and Isospin in Nuclear Interactions*, Telluride, Colorado, 1991, edited by Scott W. Wissink, Charles D. Goodman, and George E. Walker (Plenum, New York, 1991), p. 497.
[17] M. Ichimura, in *Proceedings of the Fifth French-Japanese Symposium on Nuclear Physics*, 1989, edited by K. Shimizu and O. Hashimoto (unpublished), p. 136; M. Ichimura, private communication.
[18] J.B. McClelland, T.N. Taddeucci, X.Y. Chen, W.P. Alford, R.C. Byrd, T.A. Carey, S. DeLucia, C.D. Goodman, E. Gülmez, W. Huang, B. Luther, D.G. Marchlenski, D.J. Mercer, D.L. Prout, J. Rapaport, L.J. Rybarcyk, W. Sailor, E. Sugarbaker, Y. Wang, and C. Whitten, Jr., Phys. Rev. Lett. **69**, 582 (1992).
[19] R.L. York, O.B. van Dyck, D.R. Swenson, and D. Tupa, *Proceedings of the International Workshop on Polarized Ion Sources and Polarized Gas Jets*, Tsukuba, Japan, 1990 (KEK 90-15), p. 170.
[20] M.W. McNaughton, P.R. Bevington, H.B. Willard, E. Winkelman, E.P. Chamberlin, F.H. Cverna, N.S.P. King, and H. Willmes, Phys. Rev. C **23**, 1128 (1981); M.W. McNaughton and E.P. Chamberlin, *ibid.* **24**, 1778 (1981).
[21] T.N. Taddeucci, C.D. Goodman, R.C. Byrd, T.A. Carey, D.J. Horen, J. Rapaport, and E. Sugarbaker, Nucl. Instrum. Methods A **241**, 448 (1985).
[22] J.B. McClelland, Can. J. Phys. **65**, 633 (1987); in *Proceedings of the International Conference on Spin Observables of Nuclear Probes*, Telluride, Colorado, 1988, edited by Charles J. Horowitz, Charles D. Goodman, and George Walker (Plenum, New York, 1989), p. 183.
[23] J.B. McClelland, D.A. Clark, J.L. Davis, R.C. Haight, R.W. Johnson, N.S.P. King, G.L. Morgan, L.J. Rybarcyk, J. Ullmann, P. Lisowski, W.R. Smythe, D.A. Lind, C.D. Zafiratos, and J. Rapaport, Nucl. Instrum. Methods A **276**, 35 (1989).
[24] M.W. McNaughton, I. Supek, K.H. McNaughton, K. Johnston, P.J. Riley, D.A. Ambrose, P. Coffey, G. Glass, J.C. Hiebert, L.C. Northcliffe, A.J. Simon, D. Mercer, D.L. Adams, H.M. Spinka, R.H. Jeppeson, G.E. Tripard, and H. Woolverton, Phys. Rev. C **45**, 2564 (1992).
[25] T.N. Taddeucci, W.P. Alford, M. Barlett, R.C. Byrd, T.A. Carey, D.E. Ciskowski, C.C. Foster, C. Gaarde, C.D. Goodman, C.A. Goulding, E. Gülmez, W. Huang, D.J. Horen, J. Larsen, D. Marchlenski, J.B. McClelland, D. Prout, J. Rapaport, L.J. Rybarcyk, W.C. Sailor, E. Sugarbaker, and C.A. Whitten, Jr., Phys. Rev. C **41**, 2548 (1990).
[26] D.J. Mercer, Ph.D. thesis, University of Colorado, 1992.
[27] R.A. Arndt and L.D. Roper, *Scattering Analyses Interactive Dial-In program* (SAID), Virginia Polytechnic Institute and State University (unpublished).
[28] D.V. Bugg and R.A. Bryan, phase-shift solution parametrized in the SAID program of Arndt and Roper, dated Nov. 1991 [27].
[29] T.W. Donnelly and J.D. Walecka, Annu. Rev. Nucl. Sci. **25**, 329 (1975).
[30] H. Esbensen and G.F. Bertsch, Phys. Rev. C **34**, 1419 (1986).
[31] H. Esbensen and G.F. Bertsch, Ann. Phys. (N.Y.) **157**, 255 (1984).
[32] G.F. Bertsch and O. Scholten, Phys. Rev. C **25**, 804 (1982).
[33] Richard D. Smith, in *Proceedings of the International Conference on Spin Observables of Nuclear Probes,* Telluride, Colorado, 1988, edited by Charles J. Horowitz, Charles D. Goodman, and George Walker (Plenum, New York, 1989), p. 15.
[34] Richard D. Smith and Stephen J. Wallace, Phys. Rev. C **32**, 1654 (1985).
[35] R.D. Smith and M. Bozoian, Phys. Rev. C **39**, 1751 (1989).
[36] J.M. Moss, Phys. Rev. C **26**, 727 (1982).
[37] E. Bleszynski, M. Bleszynski, and C.A. Whitten, Jr., Phys. Rev. C **26**, 2063 (1982).
[38] Munetake Ichimura and Ken Kawahigashi, Phys. Rev. C **45**, 1822 (1992); **46**, 2117(E) (1992).
[39] A.K. Kerman, H. McManus, and R.M. Thaler, Ann. Phys. (N.Y.) **8**, 551 (1959).
[40] S.A. Gurvitz, Phys. Rev. C **33**, 422 (1986).
[41] X.Q. Zhu, N. Mobed, and S.S.M. Wong, Nucl. Phys. **A466**, 623 (1987).
[42] C.J. Horowitz and D.P. Murdock, Phys. Rev. C **37**, 2032 (1988).
[43] D.V. Bugg and R.A. Bryan, Nucl. Phys. **A540**, 448 (1992).
[44] C.J. Horowitz and M.J. Iqbal, Phys. Rev. C **33**, 2059 (1986).
[45] C.W. de Jager, H. de Vries, and C. de Vries, At. Data Nucl. Data Tables **14**, 479 (1974).
[46] H. Esbensen and G.F. Bertsch, Phys. Rev. C **32**, 553 (1985).
[47] D.L. Prout, Ph.D. thesis, University of Colorado, 1992.
[48] W.M. Alberico, A. De Pace, and A. Molinari, Phys. Rev. C **31**, 2007 (1985).
[49] H. Esbensen, H. Toki, and G.F. Bertsch, Phys. Rev. C **31**, 1816 (1985).
[50] W.M. Alberico, M. Ericson, and A. Molinari, Phys. Rev. C **30**, 1776 (1984).
[51] A. De Pace and M. Viviani, Phys. Lett. B **236**, 397 (1990).
[52] T. Shigehara, K. Shimizu, and A. Arima, Nucl. Phys. **A477**, 583 (1988).
[53] G.E. Brown and Mannque Rho, Phys. Lett. B **237**, 3 (1990).